

## Localized Coupling between Surface and Bottom-Intensified Flow over Topography

ROBERT HALLBERG

*Princeton University and NOAA/Geophysical Fluid Dynamics Laboratory, Princeton, New Jersey*

(Manuscript received 11 June 1996, in final form 13 November 1996)

### ABSTRACT

Substantial bottom topography in a basin with planetary vorticity gradients strongly affects the vertical structure of the linear topographic and planetary Rossby waves that spin up the ocean circulation. There is no barotropic mode with large amplitude topography and stratification. It is shown that the lowest frequency two-layer quasigeostrophic waves that exist with stratification, planetary vorticity gradients, and large-amplitude bottom topography are more strongly concentrated in the vertical than Burger number 1 scaling would indicate (for most orientations of the wavevector) except where the bottom slope is nearly meridional. This concentration increases with decreasing frequency. Ray tracing in an ocean basin suggests that the two layers are linearly coupled in regions with parallel or antiparallel topographic and planetary vorticity gradients, but elsewhere small amplitude motion in the two layers is largely independent. Continuity within isopycnal layers implies that most of the circulation remains within isopycnal layers, even in the regions of linear coupling. The strength of surface(bottom)-intensified flow driven by coupling to bottom(surface)-intensified flow is approximately twice as strong as the surface(bottom) projection of the bottom(surface)-intensified flow. Primitive equation simulations concur with the quasigeostrophic results and indicate that the localized linear coupling between surface- and bottom-intensified flow pertains to a continuous stratification.

### 1. Introduction

Most theories of the deep circulation either describe directly forced flow (Stommel and Arons 1960; and others) or flow driven by nonlinear eddy stirring of the deep ocean (Rhines and Holland 1979). Anderson and Gill (1975) demonstrate that linear planetary waves in a flat-bottomed ocean basin tend to concentrate all of the wind-driven flow at the surface. Anderson and Kilworth (1977) extend these arguments to include meridional topography in the middle of the ocean (but still with a vertical eastern boundary and neglecting meridional variations) and find that the same result holds. Stommel and Arons prescribe the distribution of upwelling and a compensating localized source to a single active deep layer and determine the abyssal circulation this forcing implies. The circulation they find has poleward flow in the ocean interior balanced by intense western boundary currents. Kawase (1987) describes the evolution of a source-fed abyssal flow into the final state described by Stommel and Arons, and finds that most of the evolution of the flow can be described in terms of the free waves of the flat-bottom 1½-layer ocean he examines. In the present paper, it is found that the combination of large amplitude topography, stratification,

and planetary vorticity gradients causes the vertical structure of the low-frequency wave modes to change dramatically as waves propagate around an ocean basin. This changing vertical structure causes bottom-intensified flow to be driven by linear coupling with the surface circulation.

Topography can have a tremendous effect on the deep ocean response if it creates regions of closed potential vorticity (PV) contours. In the case of a source-driven flow in a 1½-layer model (with either a widely distributed sink or slow filling of the layer), Kawase and Straub (1991) find a strong cyclonic response over PV contours that are closed because of either a bottom rise or depression. Similarly, Kawase (1993) finds a very strong response to a localized mass source in a 1½-layer model with a rising bottom around the edges of a basin, compared with an analogous flat-bottom simulation, when the topography is large enough to create closed PV contours. In a multilayer quasigeostrophic simulation with topographically closed PV contours in the deepest layer, Thompson (1995) finds that a strong deep flow along the closed PV contours is excited by eddy stirring from above. Because steady flow along closed PV contours is a free mode, it is easily excited by almost any forcing, with the sense of motion determined by the forcing mechanism.

In a flat-bottomed ocean, the vertical and horizontal structure of wave modes are separable. Waves can be separated into a barotropic mode with vertically uniform horizontal velocities and countable baroclinic modes

---

*Corresponding author address:* Dr. Robert Hallberg, Geophysical Fluid Dynamics Laboratory, Princeton University, Forrestal Campus, U.S. Route 1, P.O. Box 308, Princeton, NJ 08542.  
E-mail: rwh@gfdl.gov

with zero vertical average horizontal velocities. Unfortunately, the vertical and horizontal structure of the free modes in the ocean are not separable when there is large-amplitude bottom topography. People often persist in analyzing the depth-integrated or depth-averaged velocities, even though such a field is not a dynamical mode of the system with bottom topography. This leads to the inclusion of a “JEBAR” or bottom torque “forcing” term, based on the baroclinic flow as well as the depth-averaged velocity (e.g., Mertz and Wright 1992). This term is the result of insisting on examining a field that is not a dynamical mode of the system and is not directly due to any kind of external forcing. There is no barotropic mode with stratification and topography.

The coupling between layers explored here is the direct result of the changing vertical structure of a wave mode as that wave propagates around an ocean basin. Sometimes, when the bottom slope is nearly meridional or when the wavevector is perpendicular to the isobaths, the vertical structure of the wave modes resembles that of the classic barotropic and baroclinic modes. In other places and for other wavevectors, the wave modes tend to be strongly bottom intensified or have exceedingly small velocities at the seafloor. The wave mode description of the circulation breaks down when the vertical structure changes abruptly. The changing vertical structure of a mode leads to a net horizontal transport convergence in each layer, but the resultant pressure gradients along the layer PV contours are radiated away by Rossby waves described by the other mode with a shorter timescale than the period of the waves. This coupling between the wave modes effectively keeps most of the circulation in the same isopycnal layers. Both the coupling between layers and the coupling between different wave modes occurs predominantly in the northern and southern portions of an ocean basin where the bottom slope is nearly meridional. All of the mechanisms described here apply to inviscid, adiabatic, infinitesimal amplitude circulation; no frictional or nonlinear mechanisms are evoked.

The present study uses the properties of the waves that arise in a stratified ocean with topography and planetary vorticity gradients to examine the possibility that the deep flow may be partially driven by linear coupling to the surface flow. Since no nonlinear effects are considered, the response to a change in forcing can be described as the superposition of oscillations with a continuous range of frequencies, as can be seen by Laplace transforming the linear equations of motion in time. Each of the frequencies evolves independently, so the behavior of linear waves is a strong indication of the linear, inviscid ocean dynamics.

A brief reprise of past studies of stratified topographic waves is a useful introduction to the waves examined here. Rhines (1970) examines the effect of a meridional bottom slope on the plane waves that arise in a continuously stratified fluid. On an  $f$  plane, only a single sub-inertial edge- or bottom-trapped wave mode occurs. For

sufficiently steep topography or strong stratification such that  $N \tan(\alpha)/f \gg 1$  (where  $\alpha$  is the angle between the seafloor and horizontal), this mode becomes an internal Kelvin wave (Allen 1980). At wavelengths much longer than  $(NH/f)$ , this single mode is a barotropic topographic Rossby wave. At shorter wavelengths  $L$ , this wave is a bottom-trapped topographic Rossby wave with a vertical decay scale of  $(fL/2\pi N)$ , or Burger number 1 scaling. Rotation and stratification are of equal importance for flow satisfying Burger number 1 scaling. For sufficiently long wavelengths Burger number 1 scaling gives a vertical decay scale greater than the depth of the ocean; stratification is unimportant for the dynamics of those waves. Each of these waves propagate pseudowestward (to the left of the upslope direction in the Northern Hemisphere). On a  $\beta$  plane, baroclinic Rossby waves with a horizontal velocity antinode at the surface also occur. The vertical structure of the solutions is one mode with a cosh structure (centered at the surface) and many modes with a cosine structure (also centered at the surface). With a bottom depth that decreases poleward, the planetary vorticity gradient is reinforced by the topography and the cosh mode is barotropic at long wavelengths and bottom intensified at shorter wavelengths. The gravest cosine mode is surface intensified even at the longest wavelengths. For a bottom with an equatorward upslope, the planetary vorticity gradient is opposed by the topography. For gentle topography [such that  $(\alpha f/\beta H) < 1$ , where  $\alpha$  is the slope of the bottom] the gravest cosine mode becomes barotropic at long wavelengths while the cosh mode is bottom intensified. For steeper topography the cosh mode becomes barotropic at long wavelengths while the cosine modes are surface intensified.

Straub (1994) has examined the effects of nonmeridional topography on the plane waves in a uniformly stratified ocean on a  $\beta$  plane. With nonmeridional topography, the (bottom intensified) mode with the cosh vertical structure and the (surface intensified) mode with the gravest cosine vertical structure combine to form a single, continuous mode at various orientations of the wavenumber vector. The higher cosine modes have a horizontal velocity node at the bottom, except when the flow is nearly aligned with the topography when they have an antinode. The vertical structure on either side (in wavenumber space) of the line with the antinode makes a transition of  $\pi$  in the phase of the bottom relative to the surface. (A horizontal velocity antinode is always found at the surface because of the rigid-lid approximation.) The behavior of the waves with uniform stratification, planetary vorticity gradients, and bottom topography found by Straub (1994) is qualitatively very similar to the behavior found here for a two-layer stratification.

In the present paper, the free waves that occur with arbitrarily oriented topographic gradients, stratification, and the planetary vorticity gradient are examined to determine their implications for the large-scale ocean

circulation. Models with two layers are used in this study because they are simple enough to solve for the local waves easily, but are complicated enough to capture some the leading order effects of both topography and stratification. The behavior with even this simple addition of stratification is much richer than 1/2-layer systems, where the vertical structure of the flow is specified a priori. The full range of motions pertinent to planetary scale flows with isopycnals intersecting sloping topography requires the full primitive equations. Still, most of the pertinent motions are well described by a quasigeostrophic balance, suggesting that a determination of the local dispersion relations for quasigeostrophic waves is useful. For infinitesimal perturbations to a two-layered resting fluid, these dispersion relations can easily be determined and used to trace the paths of the rays associated with the gravest waves, which spin up the steady flow. Arguments based on continuity within isopycnal layers are used to predict the strength of coupling between surface- and bottom-intensified flow and the direction of the flow driven by the coupling. The predictions from the local quasigeostrophic theory are verified with primitive equation simulations.

**2. The linear locally valid dispersion relation**

Quasigeostrophy has frequently been used to provide valuable insight into large-scale ocean motions that can only be fully described by the much more complicated primitive equations. This insight extends even to motions that clearly violate the assumptions underlying quasigeostrophy. The close correspondence between materially conserved quasigeostrophic PV and Ertel's scalar PV in the Navier-Stokes equations causes quasigeostrophic theory to apply to such large Rossby number phenomenon as fronts, isolated eddies, and instability. The atmosphere is full of large Rossby number flow, but many quasigeostrophic ideas still hold. With a layered model, quasigeostrophy requires that the topography should be small compared with the layer thicknesses. In the present case, this assumption holds only in a small horizontal neighborhood about a point. This neighborhood of validity is often smaller than the wavelength of the waves of interest! Still, the locally valid quasigeostrophic dispersion relation provides useful indications of the dynamics controlling the actual flow, as described by the primitive equations.

The linear quasigeostrophic vorticity equations for two layers are

$$\frac{\partial}{\partial t}(\nabla^2\psi_1 - \lambda_1^{-2}(\psi_1 - \psi_2)) + \beta_1 \cdot (\hat{\mathbf{z}} \times \nabla\psi_1) = 0 \quad (2.1)$$

$$\frac{\partial}{\partial t}(\nabla^2\psi_2 - \lambda_2^{-2}(\psi_2 - \psi_1)) + \beta_2 \cdot (\hat{\mathbf{z}} \times \nabla\psi_2) = 0. \quad (2.2)$$

Equations (2.1) and (2.2) suppose that there are two layers with negligibly small horizontal velocities  $\mathbf{u}_n =$

$\hat{\mathbf{z}} \times \nabla\psi_n$ , thicknesses  $h_n$ , and PVs  $q_n \approx f/h_n$ , separated by an interface with reduced gravity  $g'$ , with a rigid-lid upper surface.  $\lambda_n^2 = g'h_n/f^2$  is an internal deformation radius based on the thickness of layer  $n$ . The PV gradient times the thickness of each layer are written as  $\beta_n = h_n \nabla q_n \approx \nabla f - (f/h_n) \nabla h_n$ . In the limit of negligible velocities (and hence isopycnal slopes), the PV gradients in the two layers differ because the lower layer PV depends on the variable bottom topography.

The locally valid quasigeostrophic dispersion relation based on (2.1) and (2.2) is easily found if a wavelike structure is assumed, so that the velocity streamfunctions become

$$\begin{aligned} \psi_n(x, y, t) &= \psi_n \exp(\mathbf{k} \cdot \mathbf{x} - \omega t) \\ &\equiv \psi_n \exp(kx + ly - \omega t), \end{aligned} \quad (2.3)$$

where  $\omega$  is the frequency and  $\mathbf{k} = k\hat{\mathbf{x}} + l\hat{\mathbf{y}}$  is the horizontal wavenumber. Several definitions make the final expression for the dispersion relation and vertical structure simpler. For a total horizontal wavenumber  $K^2 = k^2 + l^2$ ,  $\omega_n = [\hat{\mathbf{z}} \cdot (-\mathbf{k} \times \beta_n)] / (K^2 + \lambda_n^{-2})$  is the frequency of Rossby waves based on the PV gradient and deformation radius of layer  $n$ . Here  $R^2 = (K^2\lambda_1^2 + 1)^{-1}(K^2\lambda_2^2 + 1)^{-1}$ , a measure of the wavelength compared with the layer deformation radii, goes from 0 (the short-wave limit) to 1 (the long-wave limit). Horizontal plane wave solutions to (2.1) and (2.2) with form (2.3) must satisfy

$$\begin{aligned} (\omega - \omega_1)(\omega - \omega_2) - (K^2\lambda_1^2 + 1)^{-1}(K^2\lambda_2^2 + 1)^{-1}\omega^2 &= 0 \quad \text{or} \\ (1 - R^2)\omega^2 - (\omega_2 + \omega_1)\omega + \omega_1\omega_2 &= 0. \end{aligned} \quad (2.4)$$

The solutions to (2.4) give the dispersion relation for horizontal plane waves

$$\begin{aligned} \omega &= \frac{1}{2(1 - R^2)}[\omega_1 + \omega_2 \\ &\quad \pm \sqrt{(\omega_1 + \omega_2)^2 - 4(1 - R^2)\omega_1\omega_2}]. \end{aligned} \quad (2.5)$$

The two solutions described by (2.5) will be referred to as the positive and negative branch of the solution depending on the sign of the radical sign. Equation (2.5) is only valid if the properties of the basin vary slowly on scales of the wavelength. Although this is not generally true in the simulations, the results of this analysis appear to make valid predictions for the full equations in a two-layer basin with large amplitude topography. The ratio of the velocity streamfunctions of the two layers associated with plane waves of frequency  $\omega$  satisfying (2.5) is

$$\begin{aligned} \psi_2 &= (K^2\lambda_1^2 + 1)(1 - \omega_1/\omega)\psi_1 \\ \text{or } \psi_1 &= (K^2\lambda_2^2 + 1)(1 - \omega_2/\omega)\psi_2. \end{aligned} \quad (2.6)$$

These equations are not novel. For example, Veronis (1980) derives essentially the same equation as (2.5) without the limitation of assuming a rigid lid. Veronis only briefly examines the effect of nonparallel topo-

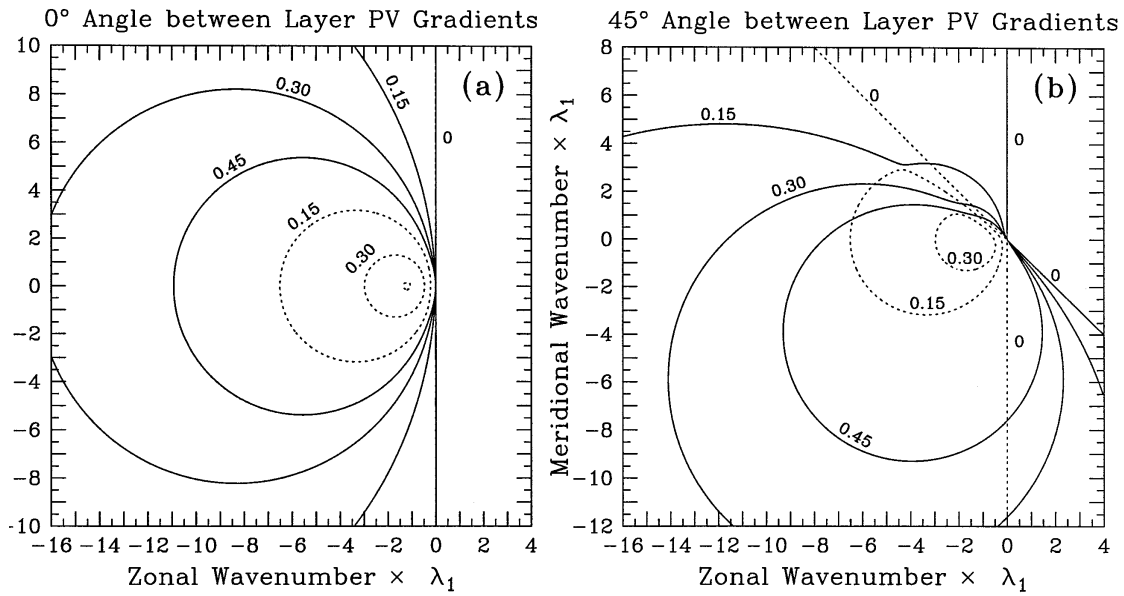


FIG. 1. Frequencies predicted by the dispersion relation, (2.5), for the lower-layer PV gradient five times as large as the upper-layer gradient and the two PV gradients are (a) parallel or (b) rotated by 45°. The negative branch of the dispersion relation is shown by dotted lines, while the positive branch is shown by solid lines. The lower layer is half as thick as the upper layer. The wavenumbers are scaled by the inverse of the upper-layer deformation radius λ<sub>1</sub>. Four equally spaced frequencies (0, 0.15, 0.3, and 0.45 β<sub>1</sub>λ<sub>1</sub>) are contoured for each branch of the solution, although in (b) the negative branch does not have frequencies as high as the largest contour value. The 0 frequency contours of the two branches coincide in (a).

graphic and planetary vorticity gradients; the added complexity that arises with nonparallel gradients makes the present study interesting.

There is some redundancy in (2.5): the same solutions are described either by considering both branches of the dispersion relation only when they have positive frequency, or by considering only one branch of the solution and retaining both positive and negative frequencies. The reason for this redundancy is that, with plane waves, the same solution is obtained if the sign of both the frequency and wavenumber are reversed. Here both branches are considered, retaining only positive frequencies. With this convention, the positive branch of (2.5) always has flow in the two layers in the same sense, while the negative branch has opposing flow in the two layers.

One interesting limit is found when planetary vorticity is held constant so that β<sub>1</sub> = ω<sub>1</sub> = 0. The two solutions to (2.5) are exactly ω = 0 and ω = ω<sub>2</sub>/(1 - R<sup>2</sup>). The zero frequency solution is a geostrophically adjusted flow with velocities entirely in the upper layer. The nonzero frequency mode is a topographic Rossby wave and has a ratio of velocity streamfunctions of

$$\Psi_1 = \Psi_2 / (K^2 \lambda_1^2 + 1). \quad (2.7)$$

This limit is revealing because the analogous continuously stratified case on an *f* plane has an exponentially bottom-trapped wave mode with a vertical decay scale given by (*fL*/*N*), where *f* is the Coriolis parameter, *N* is the buoyancy frequency, and *L* is the inverse of a typical horizontal wavenumber of the waves (Rhines 1970).

Equation (2.7) is therefore the discrete layer analog of a Burger number 1 scaling vertical structure. Coastal-trapped waves would also appear in this limit, but are excluded by the assumption of a plane wave horizontal structure and the neglect of horizontal variations in the PV gradients and deformation radii. The *f*-plane limit is also of particular interest because only topographic potential vorticity gradients can be generated using standard laboratory techniques.

The long and short wave limits are discussed by Hallberg (1995). In the short wave limit the two solutions are concentrated in one of the layers, with a frequency that is very nearly the frequency that each layer would have independently (that is ω<sub>1</sub> or ω<sub>2</sub>). In the long wave limit the two modes are a nearly barotropic mixed topographic/planetary Rossby wave and a surface (or bottom) intensified baroclinic Rossby wave closely resembling the Rossby wave in a 1½-layer model. The long wave limit is only reached for waves with very much longer wavelengths than the internal deformation radius.

At most wavenumbers, the dispersion relation gives frequencies that are either consistent with those of either bottom-trapped topographic Rossby waves (the larger set of circles in Fig. 1) or with surface-intensified planetary Rossby waves (the smaller set of circles in Fig. 1). When the layer PV gradients are parallel, the positive and negative branches of the dispersion relation each describe one of these physical modes; the circles describing the topographic waves are entirely solid lines in Fig. 1a, corresponding to the positive branch of the

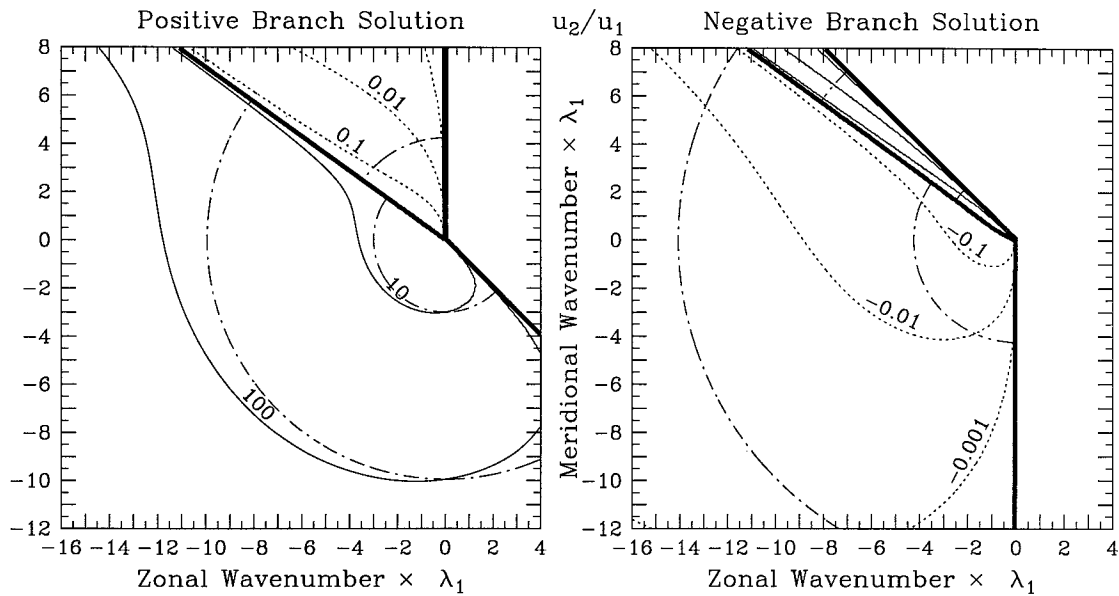


FIG. 2. The ratio of lower- to upper-layer velocities for the waves with the dispersion relation depicted in the right panel of Fig. 1. Contours indicating upper-layer intensification are dashed, while the solid contours indicate lower-layer intensification. The heavy solid lines mark equal magnitudes in the two layers. The dashed-dotted arcs mark the 100 and 10 or 0.1 and 0.01 contours given by Burger number 1 scaling. The unlabeled contours in the negative branch plot are  $-10$  and  $-100$ ; the unlabeled dotted contour in the positive branch plot is  $0.001$ .

dispersion relation, while the circles describing the planetary wave dispersion relation are entirely dotted lines, corresponding to the negative branch. However, when the upper and lower PV gradients are not parallel, both the topographic and planetary dispersion curves are described by both the positive and negative branches of the dispersion relation. This can be seen most clearly in the  $0.15 \beta_1 \lambda_1$  contours of Fig. 1b. The top-right portion of the smaller  $0.15 \beta_1 \lambda_1$  circle (describing a surface-intensified Rossby wave) is from the positive branch of the dispersion relation (a solid line), while the bottom-left portion of this circle is from the negative branch of the dispersion relation (a dotted line). Most of the larger  $0.15 \beta_1 \lambda_1$  circle (describing a bottom-intensified topographic Rossby wave) is from the positive branch (a solid line) but the portion of the larger circle inside of the smaller circle is from the negative branch (a dotted line). The simple correspondence between branches of the dispersion relation and qualitatively distinct motions when the layer PV gradients are parallel does not hold when the layer PV gradients are not parallel.

The vertical structure of the local modes also behaves quite differently between the cases where the layer PV gradients are or are not parallel. With parallel layer PV gradients the vertical structure is a function of wavelength only [in that case  $\omega_1/\omega_2$  is a function of wavelength only, and so are  $\omega/\omega_1$  and  $\Psi_2/\Psi_1$  by (2.5) and (2.6)]. By contrast, the vertical structure of the local modes is strongly dependent on the orientation of the wavevector when the layer PV gradients are not parallel, as seen in Fig. 2. Not surprisingly, at those wavenumbers

where the positive branch contours are the large circles (topographic Rossby waves) in Fig. 1b, the vertical structure of this branch is bottom intensified (solid contours in Fig. 2), while the vertical structure is surface intensified at wavelengths where this mode corresponds to planetary Rossby waves (the smaller circles in Fig. 1b). Figures 2 and 1b also show that at low frequencies, the long waves are much more surface or bottom intensified than indicated by the Burger number 1 scaling found for  $f$ -plane waves.

The positive and negative branch dispersion curves (the solid and dotted curves in Fig. 1b) osculate at regions of common wavenumber and frequency, and the branch of the solution describing the surface- and bottom-trapped mode switches, as seen by the heavy lines in Fig. 2. If there are spatial variations in the bottom slope, there can be linear coupling between the positive and negative branches of the dispersion relation at the wavenumbers where the osculation occurs. The dispersion curves at a single frequency but for angles between the PV gradients of  $35^\circ$  and  $45^\circ$  are superimposed in Fig. 3. The positive branch with a  $45^\circ$  angle and the negative branch at a  $35^\circ$  angle have essentially the same frequencies at a wavenumber of about  $(-3.5, 3)$  in Fig. 3. If locations having these angles are within a few wavelengths, the WKB approximation breaks down and the two branches of the dispersion relation can be linearly coupled. Coupling between the branches of the dispersion relation is most likely at the wavenumbers where the two branches osculate because at these wavelengths relatively small differences in the bottom slope

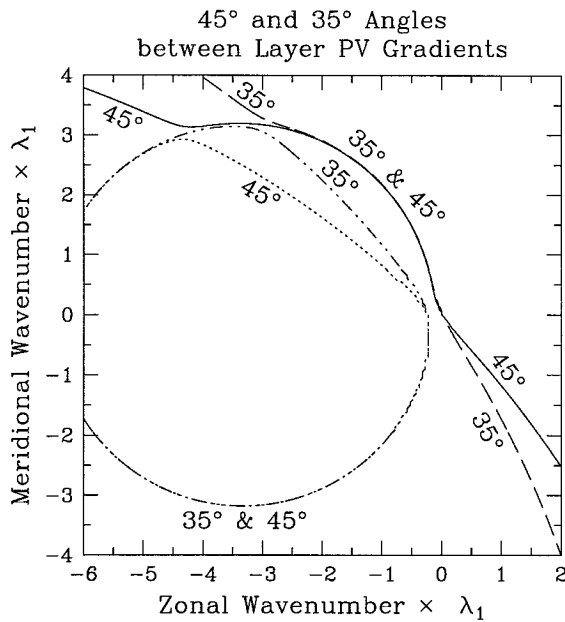


FIG. 3. As in Fig. 1 except that the domain is limited to longer wavelengths, only the  $0.15 \beta_1 \lambda_1$  contours are shown, and the fields for  $35^\circ$  and  $45^\circ$  angles between the PV gradients are superimposed. The solid and dotted lines are the contours from the positive and negative branches with a  $45^\circ$  angle between the layer PV gradients; the dashed and dashed-double-dotted lines are from the positive and negative contours with a  $35^\circ$  angle.

and orientation can cause the two branches to coincide in frequency and wavenumber normal to the gradients of the slope direction and magnitude. At the lowest frequencies and longest wavelengths, the osculation between the two branches of the dispersion relation occurs when the layer PV gradients are nearly parallel or antiparallel.

Rotating the layer PV gradients with respect to each other mimics the changes sustained by a ray as it propagates around the basin. When the two layers' PV gradients are neither parallel nor antiparallel, both branches of the dispersion relation are needed to describe either layer's mode throughout wavenumber space, as seen in Figs. 1 and 4. When the layers' PV gradients are rotated to become more antiparallel, more of the solution is described by just the positive branch of the dispersion relation, as seen in the upper panels of Fig. 4. Eventually, when the PV gradients are antiparallel, the entire solution is described by only the positive branch. As the negative branch solutions are restricted to more limited regions of wavenumber space by progressively more nearly antiparallel PV gradients, the maximum frequency obtained by the negative branch decreases.

A locally valid quasigeostrophic description leads to a relatively simple dispersion relation that describes surface-trapped planetary Rossby waves and bottom-trapped topographic Rossby waves. At certain wavenumbers, these otherwise distinct motions merge, and the branches of the dispersion relation describing each

type of motion switch. The locally valid quasigeostrophic analysis suggests the possibility of linear coupling both between surface- and bottom-intensified motions and between the two local eigenmodes, but for most orientations of the layer PV gradients and the wave vector an accurate description of the vertical modes is in terms of largely independent flow in the two layers.

### 3. Ray tracing of linear quasigeostrophic waves

Rays are a valuable tool for describing the response of an ocean basin to forcing. They indicate the pathways along which energy spreads. Also, rays indicate turning points or critical layers where energy might be focused. With the two-layer flows described here, the vertical structure of the rays is also known. Ray tracing gives a further indication of the vertical migration of energy.

The dispersion relation, (2.5), can be used for ray tracing in the two-layer basin. The ray is found by simultaneously solving the set of equations

$$\begin{aligned} \frac{Dx}{Dt} &= \frac{\partial \omega}{\partial k}, & \frac{Dy}{Dt} &= \frac{\partial \omega}{\partial l}, \\ \frac{Dk}{Dt} &= -\frac{\partial \omega}{\partial x}, & \text{and } \frac{Dl}{Dt} &= -\frac{\partial \omega}{\partial y}, \end{aligned} \quad (3.1)$$

where the material derivative is defined as the derivative following the ray (Lighthill 1978). These equations are integrated numerically. An analytically described basin shape was used so the integrations could easily be performed with arbitrarily high precision. These equations exactly conserve frequency along a ray, and this property is used to validate the numerical integration.

For the bowl-shaped basin in Fig. 5 [which is similar to that used by Hallberg and Rhines (1996) in a study of the spinup of the circulation in a basin with isopycnals intersecting the sloping topography], ray paths are calculated for a frequency of  $5 \times 10^{-8} \text{ s}^{-1}$  (Fig. 6). The internal deformation radius at the center of the basin is 77.4 km. These rays have a period of 1450 days and are sufficiently grave to be representative of the waves that spin up the steady flow following a change in the forcing (even much higher frequency rays behave similarly). The rays in this figure initially have wavelengths longer than 100 km and are uniformly distributed in wavenumber among the wavenumbers with the prescribed frequency. This choice of the initial wavenumbers ensures that all of the rays will start with a westward or pseudowestward (for topographic waves) group velocity. The starting points for the rays were chosen to illustrate the behavior of the rays throughout the basin. The density of the marks along the rays is inversely proportional to the speed of the rays, while the choice of mark indicates whether the vertical structure at that point is surface intensified or bottom intensified or neither. The dashed line in Fig. 6 marks the edge of a "forbidden region" for the negative branch rays at this frequency. Outside of this curve, all of the

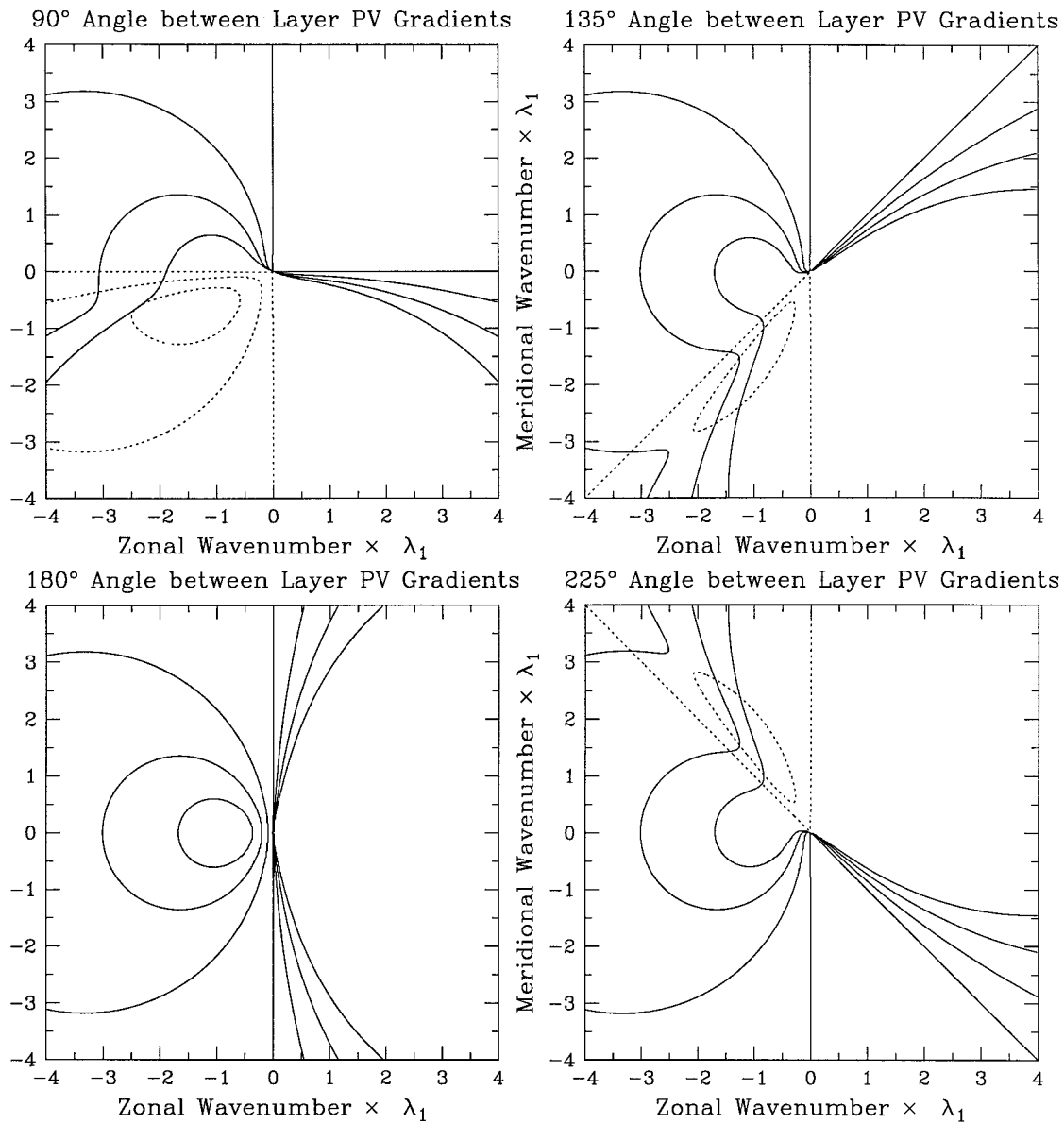


FIG. 4. As in Fig. 1 except that the region is limited to longer wavelengths and the angle between the two layer PV gradients is changed to 90°, 135°, 180°, and 225°. The same four frequencies are contoured in each panel. The positive branch of the dispersion relation is again contoured with solid lines, the negative branch with dotted lines.

negative branch solutions have lower frequency than the rays. In the south of the basin, the upper- and lower-layer PV gradients are in nearly opposite directions, and the negative branch attains only very low frequencies, as shown in Fig. 4. The positive branch rays can enter the forbidden region.

Each of the panels of Fig. 6 shows the rays spreading in two distinct groups: One group, with its signal concentrated in the upper layer, radiates nearly westward from the forcing. The other group, with its signal concentrated in the lower layer, follows the topography around the basin. Except where the planetary and topographic vorticity gradients are nearly parallel or an-

tiparallel, these low-frequency rays are much more intensified in one of the layers than would be predicted by Burger number 1 scaling. The restoring force that generates these waves is due to flow across topographic or planetary vorticity contours. The lowest frequency waves (for a given wavelength) have flow perpendicular to PV gradients and wavevectors along PV gradients. When the layer PV gradients are not parallel or antiparallel, the two layers require different orientations of the wavevector for the lowest frequency waves. Low-frequency waves accommodate these incompatible constraints on the direction of the wavevector by becoming strongly concentrated in the layer with the weaker PV

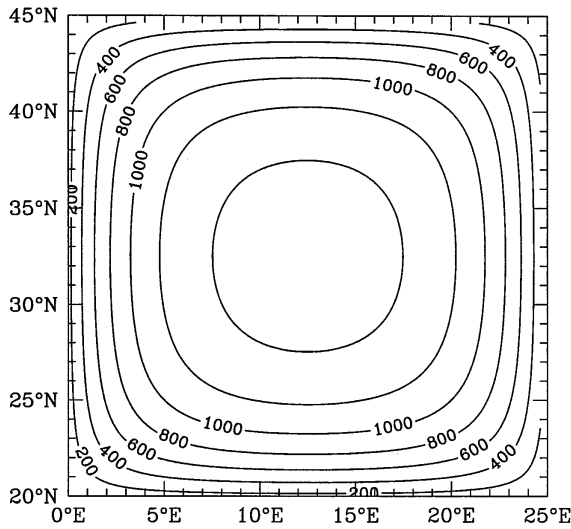


FIG. 5. Basin depth (in m) used for the ray tracing.

gradient perpendicular to the wavevector. The rays in the center of the groups are most nearly aligned with the upper- or lower-layer PV contours, have the longest wavelengths, and propagate much more rapidly than those on the edges of the group, as seen by the density of the marks in Fig. 6. The lower-layer intensified rays (which follow bottom-trapped topographic Rossby waves) generally propagate more rapidly than the upper-layer intensified rays (which follow planetary Rossby waves).

Near the forbidden region in the south, all of the rays encounter turning points. The negative branch rays cannot enter the forbidden region, so the rays approaching from the west have turning points to the west of the edge of the forbidden region and similarly negative branch rays approaching from the east have turning points to the east of the edge of the forbidden region. The positive branch rays are unimpeded by the forbidden region and have turning points inside of or even beyond the forbidden region. Lower-layer intensified rays approach the turning point from the west following the lower-layer PV contours. The rays stop and then propagate back to the west with most of their velocity in the *upper* layer instead of the lower layer. With starting points in the southeast of the basin, upper-layer intensified rays approach the forbidden region from the east, reach turning points near the forbidden region, and then propagate eastward around the basin as lower-layer waves. The symmetry between the rays with turning points in the upper and lower panels is quite striking, with one ray changing from describing surface-intensified planetary Rossby waves to describing bottom-trapped topographic Rossby waves and the other ray undergoing the opposite change in almost exactly the same place. If these rays have the same meridional wavenumber (as is indeed the case), the rays might exchange energy at their mutual turning points, with neg-

ative branch solutions interacting strongly with positive branch solutions.

In the northern part of the basin the rays also change the layer in which their motion is concentrated. This change is not associated with a turning point, as it is in the south, because the pseudowestward direction of the lower-layer intensified rays is westward with parallel topographic and planetary vorticity gradients. There is a slight change of direction as the rays are transformed because the surface-intensified rays are less tightly confined to be pseudowestward than are lower-layer intensified rays of the same frequency and wavenumber. As with the southern turning points, negative branch rays change layers before the topographic and planetary vorticity gradients are exactly parallel, while positive branch rays are transformed later.

Rays with different frequencies behave similarly to those shown in Fig. 6. Higher-frequency rays are less tightly confined to pseudowestward paths and have a larger forbidden region in the south. For frequencies low enough for planetary Rossby wave solutions to exist, the rays will all have turning points at the edges of the forbidden region in the southern part of the basin and there is localized coupling between layers in both the north and the south of the basin.

The rays shown in Fig. 6 indicate that linear coupling between the layers is localized in two regions: the northern and southern portions of the basin. This is where the topographic and planetary vorticity gradients are parallel or antiparallel. In both cases the predominant expression of a ray switches layers. This change is clearer in the south because upper- and lower-layer intensified rays propagate in opposite directions (westward and eastward, respectively). In the northern part of the basin the linear coupling is just as strongly localized, but does not appear as strikingly in the ray paths since both surface- and bottom-intensified long waves propagate westward.

The local modes in the two-layer case may not be typical in that their vertical structure is constrained by the layers. However, these two-layer solutions do illustrate the qualitative behavior of the continuously stratified case, which was described more fully by Rhines (1970) and Straub (1994) for special orientations between the bottom slope and the planetary vorticity gradient. In a continuously stratified rotating fluid, there is one mode that is bottom trapped and an infinite number of other modes in the vertical. These other modes are essentially baroclinic Rossby waves that have a horizontal-velocity node at the bottom, unless the flow is almost exactly aligned with isobaths. An important consequence of varying basin depth is that the various (locally orthogonal) modes are not globally independent, and they can exchange energy linearly.

The positive branch solution from (2.5) corresponds to the combined cosh and gravest cosine vertical structure mode found by Straub (1994) in a uniformly stratified ocean. The negative branch solution corresponds

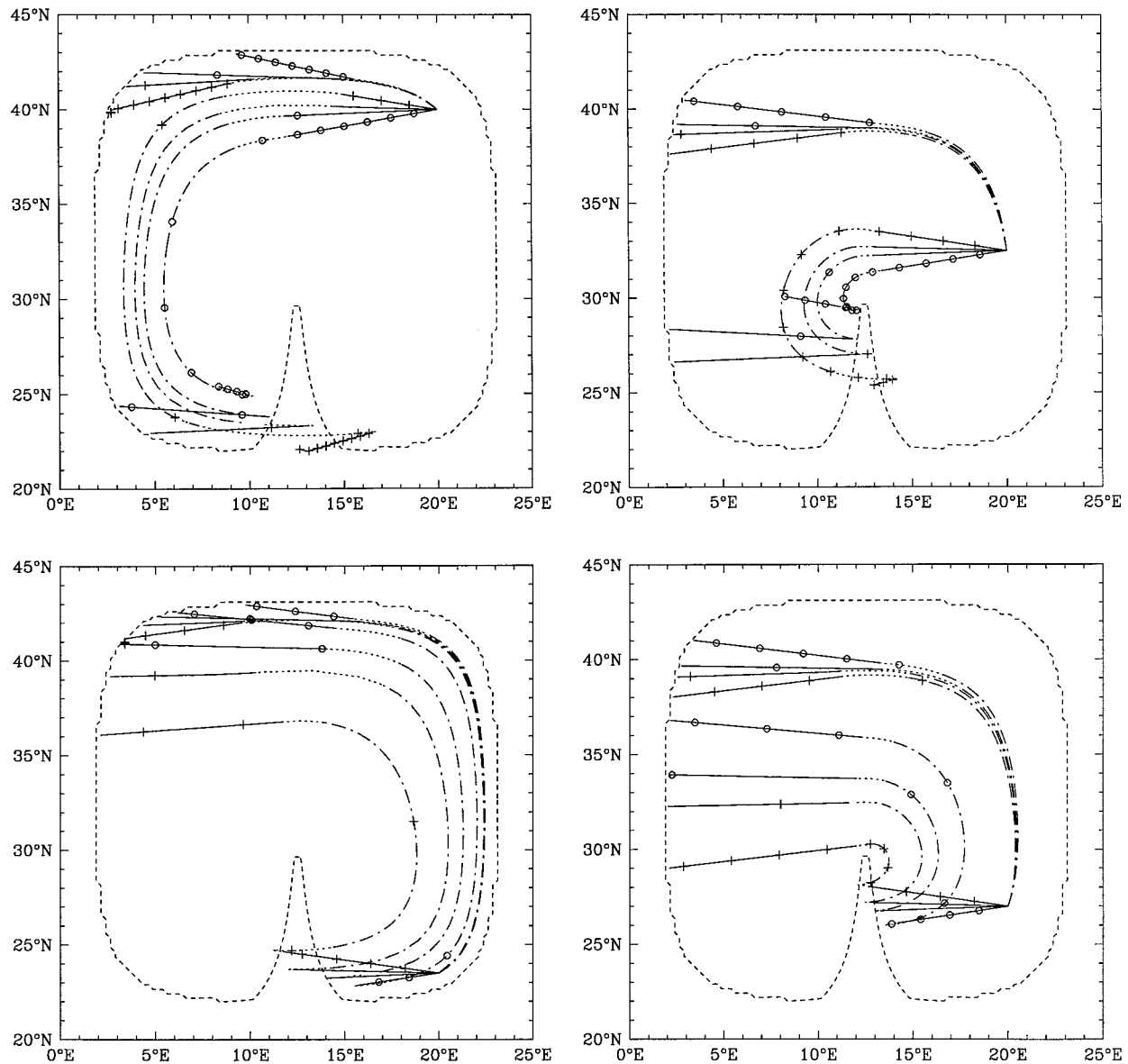


FIG. 6. Ray paths in the bowl-shaped basin for rays of frequency  $5 \times 10^{-8} \text{ s}^{-1}$ , for rays started at four locations:  $40^\circ\text{N}, 20^\circ\text{E}$ ;  $32.5^\circ\text{N}, 20^\circ\text{E}$ ;  $23.5^\circ\text{N}, 20^\circ\text{E}$ ; and  $27^\circ\text{N}, 20^\circ\text{E}$ . The line type indicates the vertical structure of the waves: A solid line is used where the rays are more than three times as surface intensified as Burger number 1 scaling would indicate; a dashed-dotted line is used where the rays are more than three times more strongly bottom-intensified than Burger number 1 scaling; and a dotted line is used otherwise. The rays go for 1500 days (or until they reach a point where the lower layer vanishes), and the position every 100 days is marked. A cross is used for the positive branch rays, while a circle is used as the mark for the negative branch rays. The dashed line around the perimeter marks the region where the maximum frequency of the negative branch is less than the frequency of the rays. The negative branch rays cannot go outside of this line.

to the first cosine structure mode with a node in the interior of the fluid. The turning points and exchange of roles between the positive and negative branch rays seen in Fig. 6 are very likely to occur in a similar way between the corresponding modes in a continuously stratified fluid. Further, the location of the coupling between surface- and bottom-intensified flow should be the same: in regions of parallel or antiparallel topographic and planetary vorticity gradients. The forbidden region in the south of the basin here will also occur in

a continuously stratified case; in the continuously stratified case the vertical structure of a mode can change abruptly as a result of changing position and wavenumber, and more vertical structure reduces the maximum frequency obtained by a mode (Straub 1994).

#### 4. The strength of coupling

There are numerous examples of physical systems with several modes of oscillation in which the energy

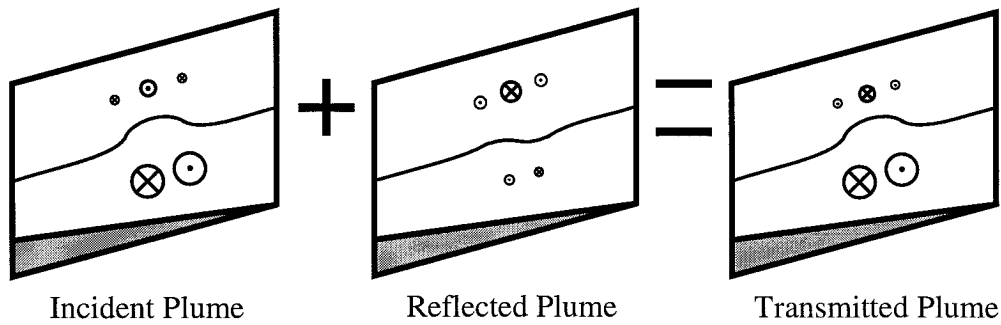


FIG. 7. Qualitative diagram of the coupling between layers and between rays for a lower-layer intensified plume with limited cross-slope extent propagating toward the southern end of a basin. The incident and reflected plumes are described by the same rays and are shown in cross sections of the flow normal to the direction of propagation taken to the west of the transition. The transmitted plume is described by a different set of rays and is shown in a cross section taken to the east of the transition. The vertical scale of the interface displacement is greatly exaggerated. The circles around crosses indicate westward flow, circles with dots indicate eastward flow. The size of the circles indicates the flow strength. North is up and to the right in each of the cross sections.

remains in one mode as the system is slowly changed and the physical expressions of the modes are interchanged. For example, Allen and Romea (1980) describe the propagation of coastal-trapped waves along the eastern boundary of an ocean. All along the coast there is a single internal Kelvin wave at a given frequency and a number of coastal-trapped waves. The mode that describes the Kelvin wave in equatorial regions describes the gravest coastal-trapped wave in midlatitudes, and Allen and Romea (1980) show that all of the energy that was in the internal Kelvin wave in equatorial regions is found in the midlatitude graves coastal-trapped wave in the limit of slow variations over the course of a wavelength. The present case does not follow this pattern of energy remaining predominantly in a single mode.

The quasigeostrophic theories neglect divergent flow relative to nondivergent flow. But in a layer with a mean PV gradient there is a net transport associated with the rotational flow. For example, Hallberg and Rhines (1996) successfully use such an argument to predict the strength of the nondivergent circulation that results from buoyancy forcing in a primitive equation numerical model. While the energy convergence in a ray within one layer can easily be balanced by time changes, dissipation, and energy flux between layers, mass flux convergence must be balanced within a layer. Even over just a fraction of a wave period, changes in layer depth cannot easily balance convergence near the edge of the domain because of the strong tendency for boundary waves to level density surfaces at the boundary (Wajsovicz and Gill 1986). If a lower-layer intensified ray propagates into a region and propagates out as an upper-layer intensified ray, the mass transport of the ray in each layer must be compensated by coupling with another ray. Arguments based on this mass transport balance can be used to provide quantitative estimates of the strength of coupling between rays and between layers.

The ray tracing of the previous section provides important clues of how the mass transports are balanced. The across-slope wavenumber was approximately conserved throughout a ray's transition from lower-layer intensified to upper-layer intensified (or vice versa). Also, for each of the negative branch rays approaching the forbidden region in Fig. 6 from one side, there is a positive branch ray of comparable cross-slope wavelength approaching from the other side, and vice versa. This suggests that a balance might be found between an incident wave in one layer, a reflected wave (on the equatorward side of the basin, or a refracted wave on the poleward side) from the same ray in the other layer, and a transmitted ray from the other branch of the dispersion relation in the first layer.

Any linear flow may be described as the superposition of waves; the spreading of a forced flow away from the forcing follows the linear waves. The vertical structure of the flow is determined by the free waves that constitute the flow, and coupling between layers is caused by migration of the energy of the free waves from one layer to the other. The envisioned mass transport balance for a plume propagating across a slope is qualitatively illustrated in Fig. 7. The arguments that follow describe coupling between waves, but apply equally to any linear, locally unforced motion.

The net transport in each layer is proportional to the strength of the rotational flow in each layer times the ratio of the PV difference between opposed jets to the mean PV between the jets (Hallberg and Rhines 1996). The three waves have the same cross-slope structure, so this constant of proportionality in each layer is the same for all three waves and drops out of the problem. Suppose that the lower layer cross-slope velocity structure is the same in each layer, save for a scaling factor  $\Psi_I$ ,  $\Psi_R$ , or  $\Psi_T$  for the incident wave, reflected wave (described by the same rays as the incident wave), and transmitted wave (with all of the rays in the incident wave replaced by rays from the opposite branch of the

dispersion relation). The upper-layer cross-slope velocity structure of the three waves will also be similar, but with different scaling factors. If the incident wave is concentrated in layer 2, with an expression in layer 1 that is weaker by a ratio  $r_I$ , while the reflected wave is expressed more strongly in layer 1 by a ratio  $1/r_R$ , and the transmitted wave is expressed more strongly in layer 2 by a factor of  $-r_T$ , the mass transport balances within the two layers at a turning point are

$$r_I\psi_I + \psi_R/r_R = -r_T\psi_T \quad (4.1)$$

$$\psi_I + \psi_R = \psi_T \quad (4.2)$$

for layers 1 and 2. The ratios  $r$  are either all less than 1 in magnitude (if the incident wave is bottom intensified) or all greater than 1 in magnitude (if the incident wave is surface intensified) and are either all positive or all negative by construction. Equations (4.1) and (4.2) are easily solved for the ratios of the streamfunctions, giving

$$\frac{\psi_R/r_R}{\psi_I} = -\frac{r_I + r_T}{1 + r_R r_T} \quad \text{and} \quad \frac{\psi_T}{\psi_I} = \frac{1 - r_I r_R}{1 + r_R r_T} \quad (4.3)$$

when the topographic and planetary vorticity gradients are antiparallel.

If the case at the poleward side of the basin is considered, the incident ray does not encounter a turning point, and the “reflected” wave terms in (4.1) and (4.2) must be moved to the right-hand side of the equations (and reinterpreted as “refracted” wave terms). When the topographic and planetary vorticity gradients are parallel, the ratio of the streamfunctions are

$$\frac{\psi_R/r_R}{\psi_I} = \frac{r_I + r_T}{1 + r_R r_T} \quad \text{and} \quad \frac{\psi_T}{\psi_I} = \frac{1 - r_I r_R}{1 + r_R r_T}. \quad (4.4)$$

The ratios  $r$  are typically of comparable magnitude and much less than 1 for low-frequency bottom-intensified waves or much greater than 1 for low-frequency surface-intensified waves. With this assumption, the transmitted wave has velocities of comparable magnitude to those of the incident wave, while the reflected wave’s velocities are smaller by a factor of  $r$ . For the rays depicted in Fig. 6, which have values of  $r$  of order 0.05, the ratios of the reflected to incident streamfunctions (in the layers in which the rays are intensified) and transmitted to incident streamfunctions for the transition in the south are about 0.1 and 0.995.

The relative sense of the incident waves determines the sense of both the circulations they excite. The incident and transmitted waves have the same sense of circulation in the layer in which they are concentrated, but the opposite sense in the other layer. The incident and reflected (or refracted) waves (which are on the same ray, and are described by the same branch of the dispersion relation) have circulation in the opposite sense in both layers near a turning point (where the topographic and planetary vorticity gradients are anti-

parallel), but in the same sense when the topographic and planetary vorticity gradients are parallel.

The extent of coupling between layers is strongly dependent on the frequency and scale of the motion. As seen in Fig. 2, higher-frequency rays tend to be less strongly localized in one layer and will exhibit stronger coupling between layers than will lower-frequency waves. The region of coupling is also less localized for higher-frequency waves. For there to be any coupling at all, though, the frequency must be less than the maximum frequency for internal planetary Rossby waves. Above this frequency there are no surface-intensified waves. Longer waves are also less strongly localized in one layer than are shorter waves and will exhibit stronger coupling between layers. Intimately tied to the coupling between layers is coupling between the vertical eigenmodes; coupling between the modes is responsible for flow that remains surface or bottom intensified while the linear waves change the layer in which they are expressed.

### 5. Localized layer coupling in primitive equation simulations

The possibility of localized coupling between bottom-trapped motion and surface-intensified motion in a basin with large amplitude topography, as is suggested by the ray tracing, can be examined with primitive equation model simulations. The ray tracing is based on the validity of the local quasigeostrophic representation of the flow, but the WKBJ approximations are clearly not justifiable in this case. The predictions of ray tracing arguments are often borne out, even though the WKBJ approximation leading to the ray tracing is not valid. By contrast, all of the assumptions leading to the primitive equations are clearly valid for the large-scale motions of interest.

One difficulty with using primitive equation simulations to explore the possibility of localized coupling is that the wide range of motions are difficult to distinguish and the cause of those motions is difficult to determine. In this section, several simulations that attempt to clearly separate different sources of motion are presented. These simulations are initially at rest, and the response to the impulsively applied forcing is transmitted around the domain by the linear topographic and planetary Rossby waves discussed before. The coupling between layers indicated by the ray tracing is evident in the evolution of these spinup simulations.

First, two-layer simulations are used for simplicity and for direct comparison with the quasigeostrophic results from section 3. Next a four-layer simulation is presented to demonstrate that the two-layer results are qualitatively pertinent to an ocean with more general stratification. The primitive equation model used is described in the appendix of Hallberg and Rhines (1996) and in more detail in Hallberg (1995). The ray tracing suggested that coupling between layers occurs in lo-

calized regions, and the primitive equation experiments are found to support this hypothesis.

*a. Two-layer simulations*

The possibility that flow in one layer forces distinct motions in the other layer is examined with a pair of bowl-shaped basins set into a zonally reentrant channel.

The topography, shown in Fig. 8, is flat at the depth of the interface between the layers, 750 m deep, while the lower layer is entirely contained within the bowl-shaped basins. The reduced gravity of the interface between the layers is the same as in the ray tracing calculations. The upper-layer PV contours are zonal, and the motions in the upper layer are largely confined to the latitudes at which they are generated. The simulations are forced

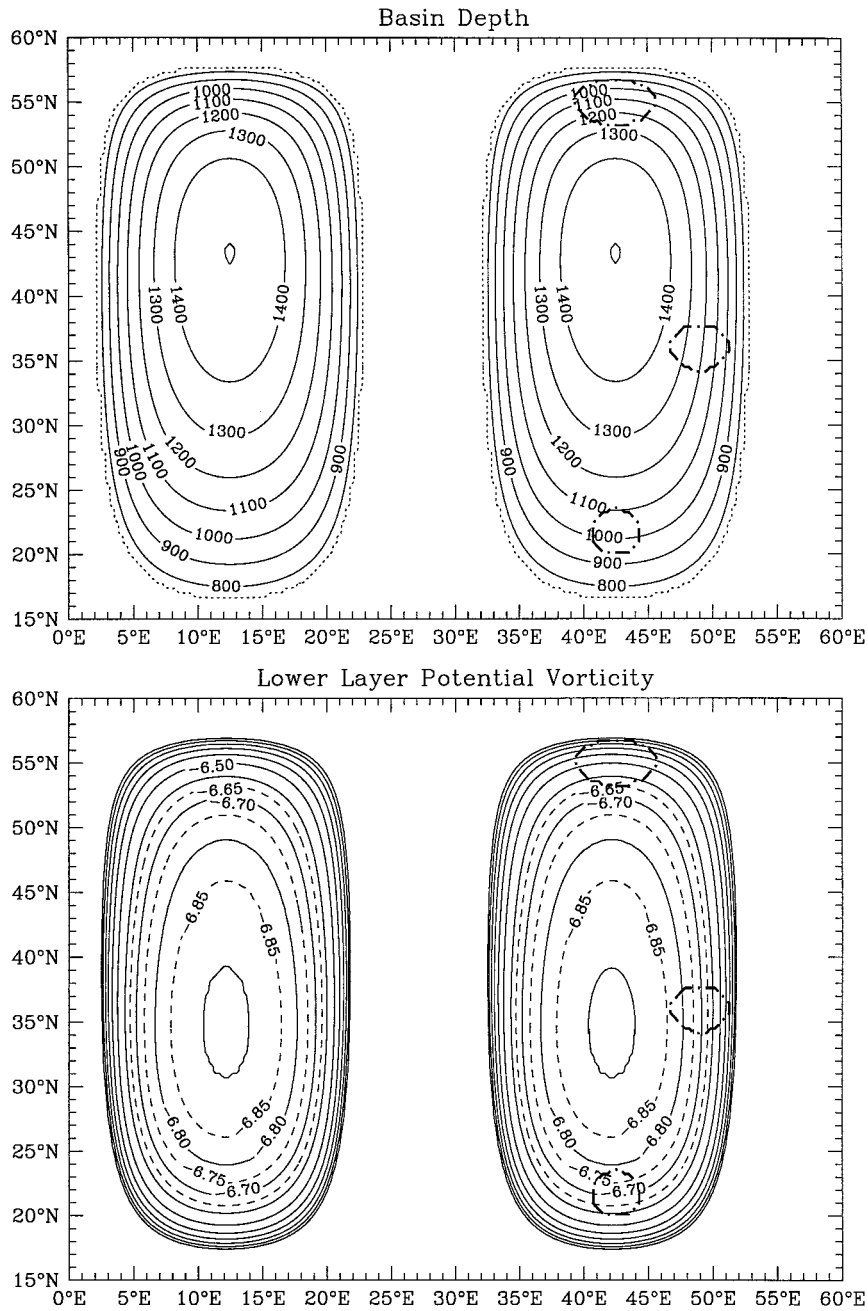


FIG. 8. The basin depth (in m) and  $\log_{10}$  of the initial lower layer PV (in  $\text{m}^{-1} \text{s}^{-1}$ ) for the experiments demonstrating coupling between the layers. The dashed-dotted circles mark the forcing regions. The upper layer has a uniform depth of 750 m; the 750-m depth contour is marked by the dotted line in the upper panel.

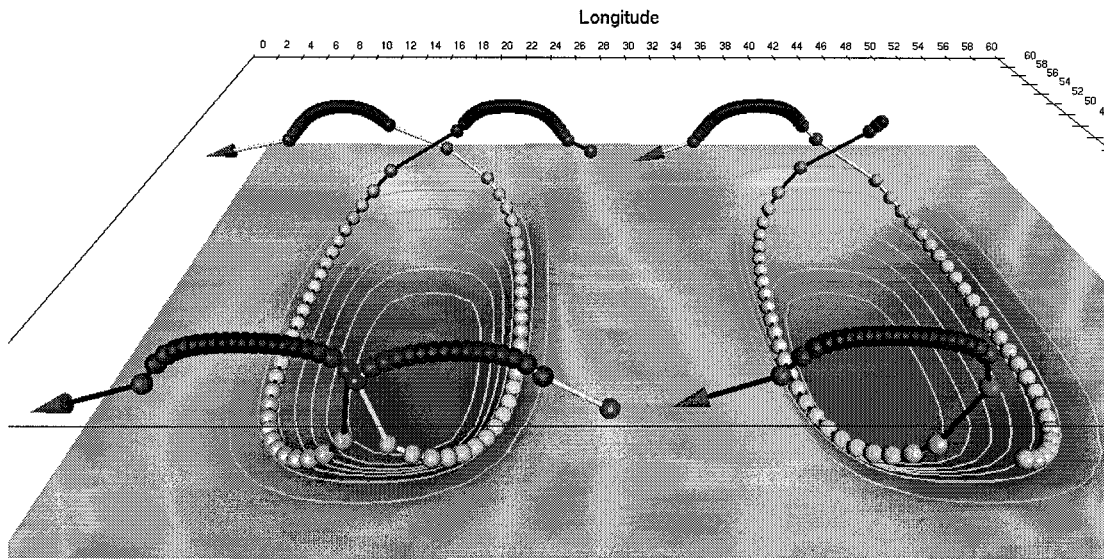


FIG. 9. Selected ray paths showing the propagation of information in the channel with two basins shown in Fig. 8. The balls mark the ray position every day. The color of the ball and the vertical position indicate the vertical structure of the rays. Surface-intensified rays have dark balls and are plotted near the surface; bottom-intensified rays have light balls and are plotted near the bottom. The ray is in the middle of the upper layer when the magnitude of the flow in the two layers is equal. The connecting lines are white or black all along a ray.

by a uniform intensity transfer of mass from the upper layer to the lower within one of the regions marked by dashed-dotted contours in Fig. 8. The forcing is sufficiently weak that the flow is well described by linear dynamics. The lower-layer signals propagate around the basin following the lower-layer PV contours, shown in the lower panel of Fig. 8, while upper-layer intensified signals propagate along the zonal upper-layer PV contours. The topography in these large basins is much steeper in the north than the south so that the lower-layer PV gradients in the north and south are of comparable magnitude.

The propagation of waves around these basins is illustrated in Fig. 9. The vertical structure is indicated by the vertical position of the rays. The transitions of a ray between describing upper- and lower-layer intensified flow are clearly visible in the northern and southern ends of the basins (where the topographic and planetary vorticity gradients are aligned). Elsewhere in the basins, the rays are extremely surface or bottom intensified. Where the rays cross (in the north) or osculate (in the south) there is strong coupling between rays, as discussed in section 4. All of the rays in Fig. 9 are from the positive branch of the dispersion relation, and between the two basins these rays describe barotropic waves (there is only one layer outside of the basins). In the primitive equation experiments, the forcing excites the rays where they pass through the northern or southern end of the eastern basin.

These experiments are designed to clearly demonstrate the coupling between layers. The basin itself is large enough to physically separate the upper- and low-

er-layer signals. The distinct meridional separation between the directly forced beta-plume in the upper layer (the response to the forcing in a reduced gravity model of the upper layer alone) and the hypothesized coupling driven flow makes the forcing of upper-layer flows by the lower layer particularly clear. Without coupling between the layers, lower-layer flow would be confined to the easternmost of the two basins, while the upper-layer flow easily propagates westward over the western basin. Any lower-layer flow in the unforced basin must be the result of upper-layer motions exciting lower-layer flows.

When the forcing is in the north, the directly forced upper-layer beta-plume is confined north of about  $45^{\circ}\text{N}$ , as seen in Fig. 10. There is also a weak upper-layer flow above and parallel to the directly forced lower-layer topographic beta-plume. The vertical scale of the bottom-trapped flow is much smaller than Burger number 1 scaling (which suggests that  $H = fL/N$ ) would predict, in agreement with the findings from the ray tracing in section 3, and with the findings of Straub (1994) based on his study of linear quasigeostrophic motion on a linearly stratified  $\beta$  plane with topography. This motion is not indicative of coupling between the motions concentrated in the two layers; it is part of the same locally defined vertical mode as the lower-layer flow. It spins up following the lower-layer PV contours. Both the directly forced upper-layer beta-plume and the upper-layer expression of the lower-layer intensified flow are analogous to flows that develop with purely meridional bottom slopes and no coupling between modes.

In the southern part of the basin, there is a distinct type of motion in the upper layer, as seen in Fig. 10.

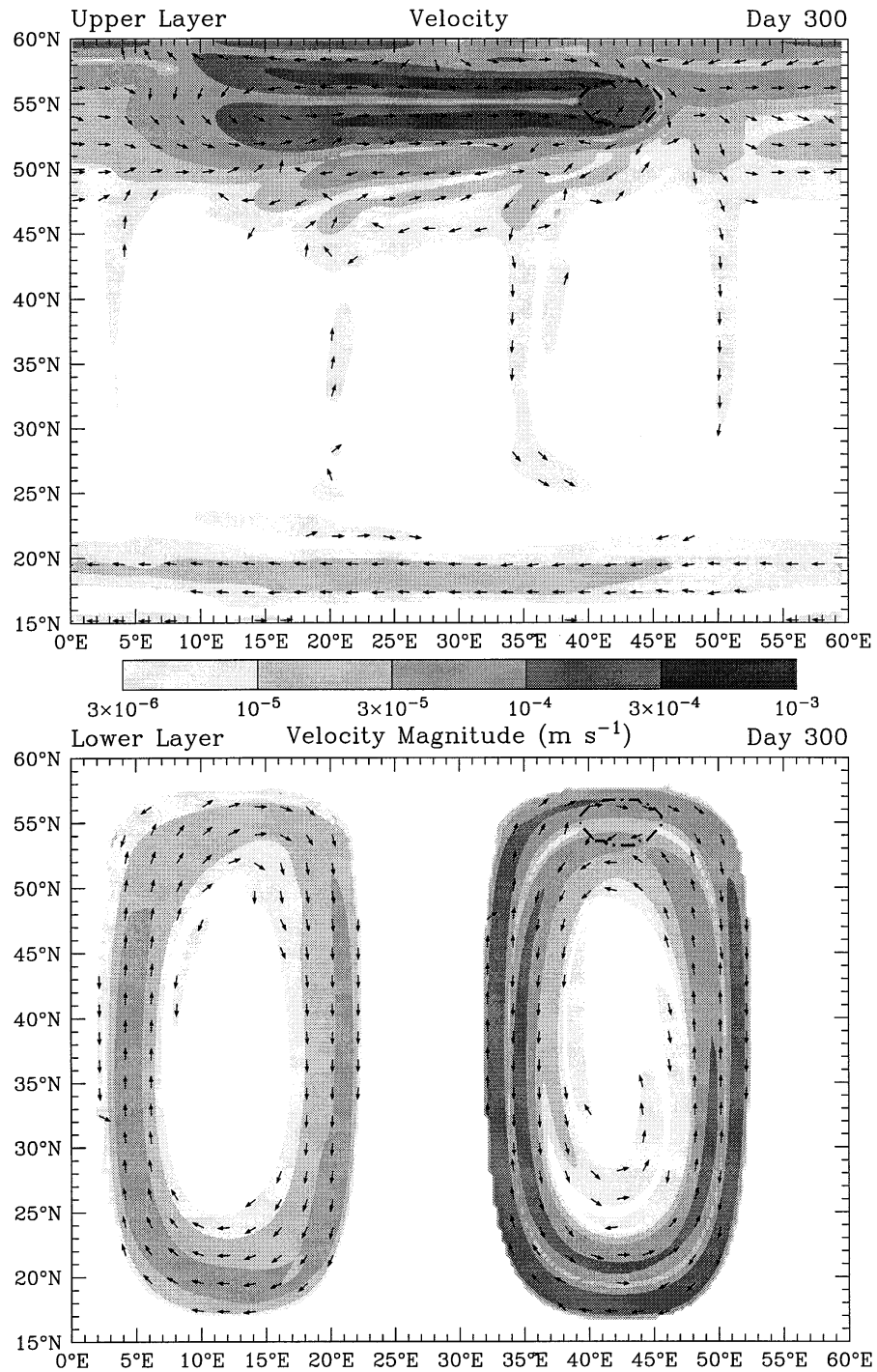


FIG. 10. The magnitude of the velocities in a reentrant channel at day 500 due to forcing in the north of the eastern basin, marked by the dashed-dotted circle. The arrows indicate the sense of the flow.

This circulation is upper-layer intensified and propagates westward following the upper-layer PV contours, but this flow does not originate in a region of external forcing. Neither is it the upper-layer expression of lower-layer intensified flow since the upper-layer flow ex-

tends westward past the edge of the lower layer. This upper-layer circulation is forced by coupling between the layers. The ray tracing in section 3 suggested that the coupling between the layers should be localized in the south of the basin, where the topographic PV gra-

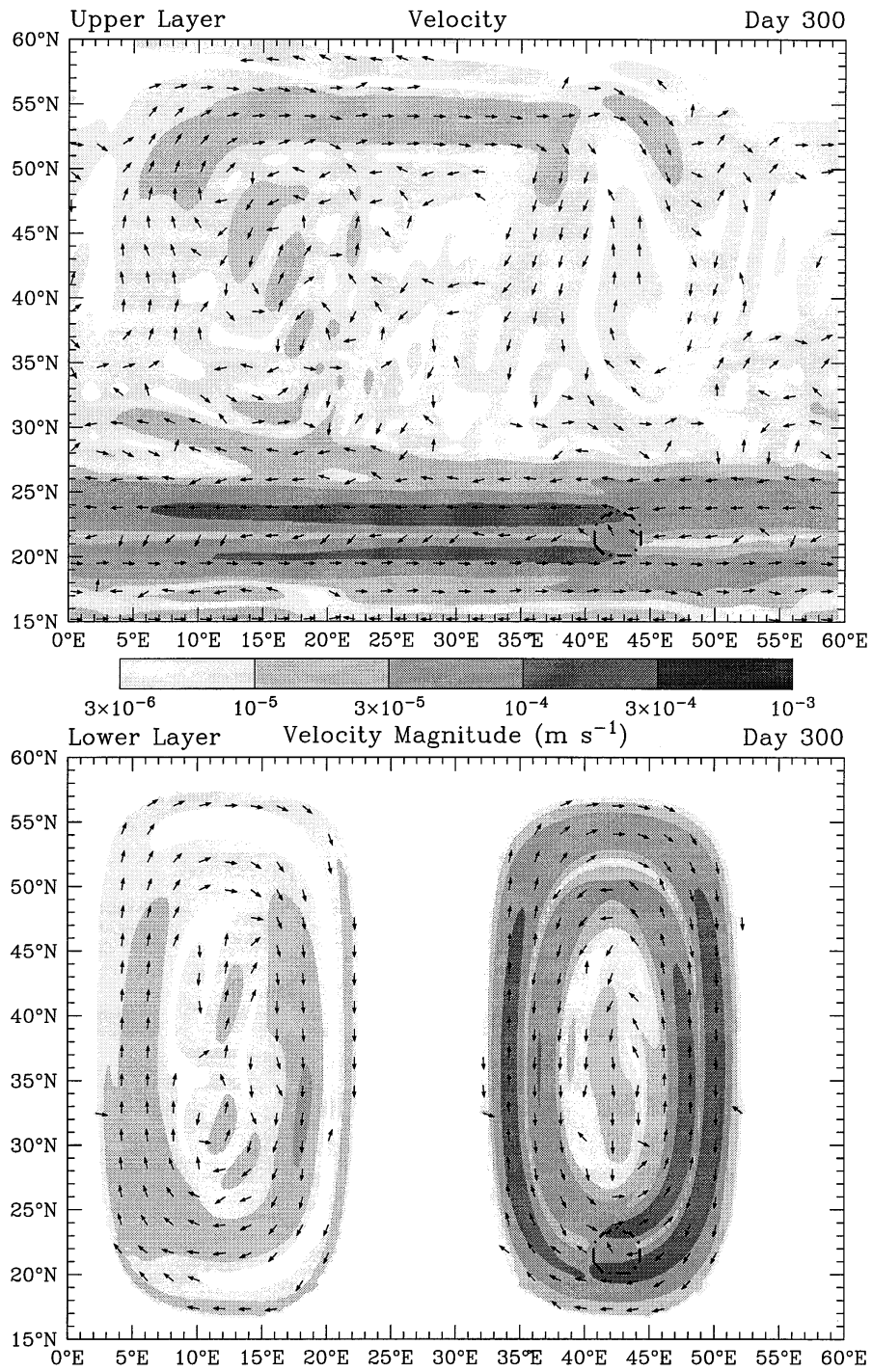


FIG. 11. The magnitude of the velocities in a reentrant channel at day 500 due to forcing in the south of the eastern basin, marked by the dashed-dotted circle. The arrows indicate the sense of the flow.

dient is antiparallel to the planetary vorticity gradient, and in the northern part of the basin, where the topographic PV gradient is parallel to the planetary vorticity gradient. No upper-layer flow radiates westward from the eastern basin except the directly forced beta-plume in the north and the weaker flow in the south, suggesting

that the coupling between layers does not take place along the eastern or western sides of the basin.

With forcing in the south, coupling in the northern part of the channel is clearly visible. The upper-layer velocity, Fig. 11, shows an upper-layer flow extending westward from the northern end of the basin. With a

more equatorial forcing in this case, the larger Rossby radius leads to much more dispersion of the directly forced beta-plume, and the flow forced by coupling between the layers is more difficult to discern. Still, the apparent upper-layer response is in the location indicated by the ray tracing. In neither the simulation forced in the north nor the simulation forced in the south is there any indication of linear coupling from the lower layer to the upper except where the upper- and lower-layer PV gradients are nearly parallel (in the north) or antiparallel (in the south).

The three forcing locations are used to test coupling from the upper layer to the lower. These forcing locations generate upper-layer beta-plumes that cross the unforced western basin either in the north, in the south, or through the middle of the basin. The ray tracing suggested the possibility of strong linear coupling in the south and north, but weak (or no) linear coupling along the eastern and western walls. If this description is correct, the cases forced in the north and south, shown in Figs. 10 and 11, should show strong flow around the edges of the unforced basin, while only the very center of the unforced basin should respond to an upper-layer beta-plume crossing the middle of the unforced basin. Comparison of Fig. 12 with Figs. 10 and 11 reveals that this is true. The magnitudes of the maximum velocities in the lower layer in the unforced (western) basin in all three cases are comparable, about  $10^{-4} \text{ m s}^{-1}$ , but the maximum velocities are clearly concentrated around the edges of the basin in Figs. 10 and 11, while in Fig. 12 the maximum velocities are concentrated in the middle of the basin.

That there is any motion in the lower layer of the unforced basin is an obvious indication of the linear coupling between upper- and lower-layer intensified motions with large amplitude topography. In the cases where the forcing comes from an upper-layer plume crossing either the northern or southern portions of the basin, it is not surprising that the response is strongly concentrated near the margins of the basin. The lower-layer intensified flow is concentrated on the coupling-forced PV contours, and these contours are primarily dictated by the topography. The support for the idea that the coupling between the layers is localized in regions of parallel or antiparallel layer PV contours comes from the case where the upper-layer flow crosses the middle of the basin. The region of parallel or antiparallel layer PV contours extends meridionally through the middle of the basins. All of the lower-layer PV contours in the unforced basin are crossed by the upper-layer flow, but only the PV contours in the middle of the basin exhibit a strong response. The upper-layer flow is broad enough that it extends into the regions of parallel and antiparallel PV contours near the middle of the basin, and these are the PV contours which develop a circulation.

The arguments of section 4 predict the sense of the circulations driven by the coupling between the layers. All of the mechanisms presented here are linear, and

reversing the sense of the forcing reverses the sense of the flow everywhere.

The two-layer primitive equation model experiments described here clearly demonstrate that the upper- and lower-layer intensified motions are linearly coupled. They further indicate that this coupling is localized near regions of parallel or antiparallel planetary and topographic PV gradients, in concurrence with findings from the quasigeostrophic ray tracing described in section 3. Based on the strength of the flows driven by coupling between layers in the primitive equation simulations, the coupling causes on the order of 1% of the energy to change layers in the regions of parallel or antiparallel planetary and topographic PV gradients. This strength of coupling agrees well with the arguments of section 4.

#### *b. A four-layer simulation*

Coupling between surface-intensified flow and bottom-intensified flow should occur in the case of a continuously stratified ocean as well. In a continuously stratified ocean with nonmeridional topography, the same local mode describes bottom-trapped motion and surface-trapped motion with no horizontal velocity nodes (Straub 1994). The next mode has a cosine structure with one horizontal velocity node, but the structure changes from having that node on the bottom to having the node in the interior and almost a second node at the bottom; that is, the phase difference between the top and bottom changes by almost  $\pi$  for different orientations of the wavevector. The next mode still has two nodes but almost attains a third for some wavevector orientations (Straub 1994). Each of the cosine modes osculates to the next higher cosine mode for wavevectors nearly aligned with the topography, where the wavenumber, frequency, and vertical structure of subsequent modes is nearly identical. It is reasonable, then, to expect that each of the vertical local modes in the uniformly stratified ocean will be coupled with the next mode. It is also reasonable to expect that the strongest coupling between the uniformly stratified modes might be localized in the same regions as the coupling between the two-layer modes—namely, in regions of parallel or antiparallel topographic and planetary vorticity gradients.

The prediction that the various vertical modes in a continuously stratified ocean are coupled in regions of parallel or antiparallel topographic and planetary vorticity gradients can also be tested with primitive equation simulations. With four layers, there are three modes with a horizontal velocity node at the bottom in addition to the bottom-intensified topographic mode for most orientations of the wavevector. In this simulation the reduced gravity of each internal interface is half the value used in the preceding two-layer simulations. The bottom topography, shown in Fig. 13, is flat at the level of the interface between the second and third layers except in a bowl-shaped basin, and the domain is zonally reentrant.

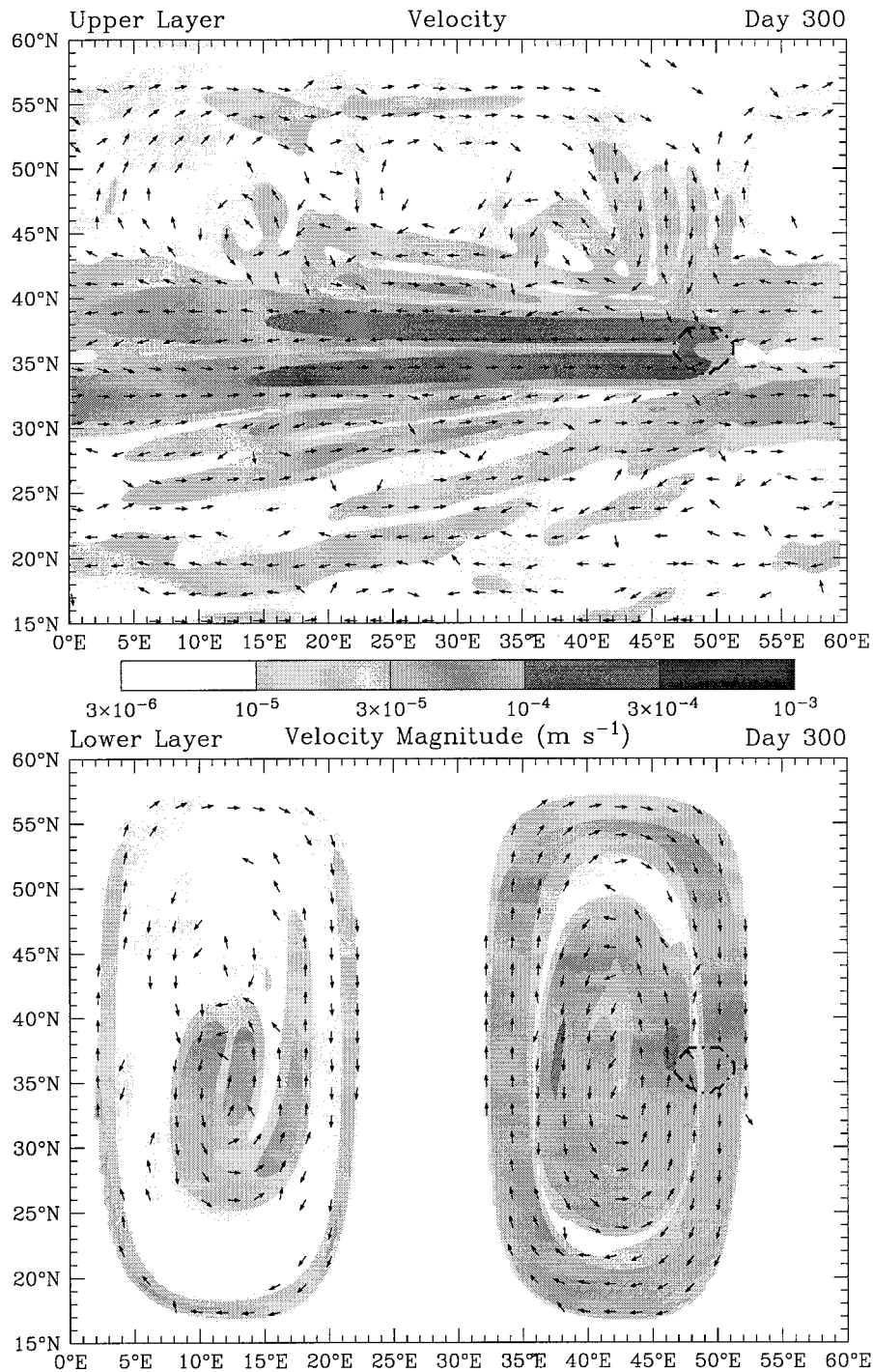


FIG. 12. The magnitude of the velocities in a reentrant channel at day 500 due to forcing in the east of the eastern basin, marked by the dashed-dotted circle. The arrows indicate the sense of the flow.

The thickness of each layer is initially a quarter the maximum basin depth. Over the flat bottom the only vertical modes are the classic barotropic and first baroclinic modes.

The buoyancy forcing, over the flat bottom just to the east of the basin, projects almost entirely onto the first

baroclinic mode. It takes about 700 days for the baroclinic beta-plume generated by the forcing to reach the eastern edge of basin. By this time, the weaker direct barotropic response from the forcing has spread throughout the domain. Along the northern portion of the basin, the baroclinic beta-plume is coupled with the

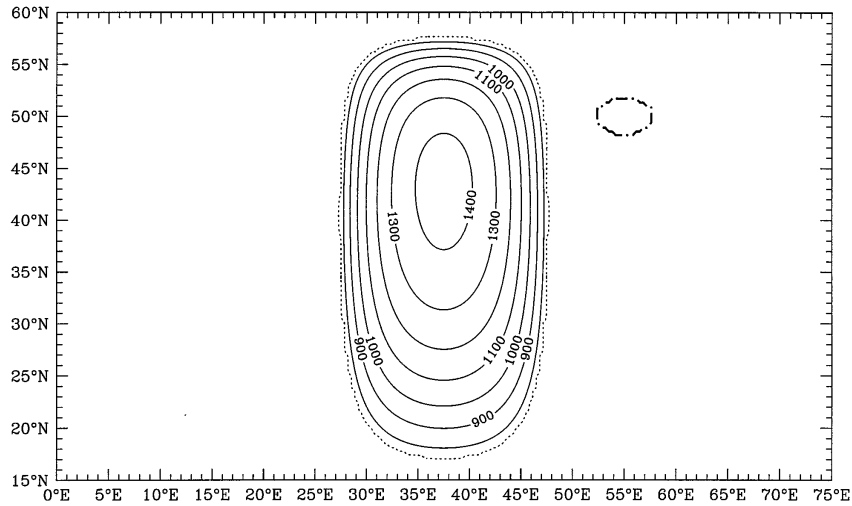


FIG. 13. Basin depth, in m, for the four-layer simulation. The dashed-dotted circle marks the forcing location.

bottom-intensified flow and with the graver surface-intensified mode. The coupling between surface-intensified modes is evident in the first panel of Fig. 14 in the strong circulation extending westward from the northeastern portion of the basin, rather than from the forcing region. The lower layers are driven by coupling with the surface circulations in the north of the basin and propagate quickly around the basin. The velocities in the lower layers are roughly a tenth as large as the baroclinic velocities in the baroclinic circulation to the east of the basin; the barotropic velocities to the west of the basin are similarly of order a tenth as strong as the directly forced baroclinic flow. In the south of the basin, the bottom-trapped flow drives surface-intensified flow. Figure 14 shows both barotropic and baroclinic signals radiating westward from the southern end of the basin. Again, the surface intensified flow in the south has velocities about a tenth as large as the lower-layer velocities that drive them. This primitive equation simulation strongly suggests that the surface- and bottom-intensified flow are linearly coupled in regions of parallel or antiparallel topographic and planetary vorticity gradients with a continuous stratification, as well as in the case of homogenous layers with abrupt density gradients.

## 6. Conclusions

Linear waves are relevant to the dynamics of the flow in an ocean basin because they determine how the ocean circulation responds to changes in forcing. Large amplitude topography greatly complicates linear Rossby waves by creating mixed topographic-planetary waves. The circulation in a basin with large amplitude topography can be decomposed locally into vertical modes, but these modes are linearly coupled if the orientation of the bottom slope varies. These modes do not cor-

respond to the classic barotropic and baroclinic modes when there is a sloping bottom, and their vertical structure depends strongly on the orientation of the wavevector when the bottom slope is not purely meridional. A local quasigeostrophic representation of the flow in two layers with bottom topography and planetary vorticity gradients is used to examine the interaction between layers in planetary-scale flows. The resulting dispersion relation is the solution to a quadratic equation and consists of two branches. The local dispersion relation shows that when the planetary and topographic vorticity gradients are not exactly parallel, upper- and lower-layer intensified waves are both described by both branches of the dispersion relation. Put differently, the gravest surface intensified planetary Rossby wave and the topographic Rossby wave are actually a part of the same mode, while the next gravest vertical mode can predominantly describe either surface or bottom flow. The low-frequency waves tend to be much more vertically concentrated than would be indicated by Burger number 1 scaling. The exception to this enhanced vertical intensification is for wavevectors where the topographic and planetary PV gradients have comparable projections normal to the wavevector. At these wavenumbers the two wave modes osculate with one another. For parallel layer PV gradients, the two branches describe the classic barotropic baroclinic modes. When the layer PV gradients are antiparallel, the entire dispersion relation is described by just one branch of the dispersion relation.

The locally valid dispersion relation for two layers in a basin with topography is used to trace groups of rays with a specified frequency starting from the same point. These low-frequency rays spread from the source in two distinct groups; one group is strongly upper-layer intensified and heads generally westward, nearly tangent to the upper-layer PV contours, while the other group

circles the basin along the lower-layer PV contours. Both groups of rays comprise rays from both of the branches of the dispersion relation. As a ray propagates, it encounters changing layer thicknesses and bottom slopes, and its projection onto the two layers changes. Eventually the rays reach a point in the basin where the two branches of the dispersion relations osculate to each other. At this point the modes are linearly coupled, and energy is freely exchanged. A single ray can change from being primarily expressed in one layer and following that layer's PV contours to being primarily expressed in the other layer and following its PV contours. This change can happen quite suddenly at turning points where the topographic and planetary vorticity gradients are in opposite directions, or more gradually where the two gradients are aligned, and provides a linear mechanism for coupling between the two layers' flows. The ray tracing suggests that the most intense coupling of low-frequency surface- and bottom-trapped waves is localized in regions of nearly parallel or antiparallel planetary and topographic vorticity gradients. This localization is especially acute for very low frequencies.

The coupling between surface- and bottom-intensified flow is due to the changing vertical structure of the wave modes as they propagate around an ocean basin. Where the coupling occurs, the wave modes resemble the classic barotropic and baroclinic modes, which have significant expression throughout the water column. Elsewhere, the wave modes are surface or bottom intensified.

The linear coupling between surface- and bottom-intensified flows only occurs when large amplitude topography, the planetary vorticity gradient, and stratification are all taken into account. Without bottom topography the vertical and horizontal structure of the planetary waves are separable, and the textbook case of linearly independent barotropic and baroclinic vertical modes is found. In the absence of planetary vorticity gradients, the only solution with nonzero frequency is bottom-intensified (or barotropic) topographic Rossby waves. Of course, if density stratification is neglected, there is only a single vertical mode, which has a dispersion relation set by a simple combination of the topographic and planetary vorticity gradients. The coupling between surface- and bottom-intensified flow, described in the present study, arises from the complex interplay of large amplitude topography, stratification, and the planetary vorticity gradient in determining the dynamics of the free waves.

Experiments with a numerical primitive equation model confirm the hypothesized spatially localized coupling between surface- and bottom-intensified flow in regions of parallel and antiparallel planetary and topographic vorticity gradients. These experiments demonstrate that energy can pass either upward or downward in such places. By definition rays cannot split, but there is no such constraint on the energy. There is a net mass transport associated with a ray within each layer, but

persistent horizontal convergence is not sustainable. Topographic or planetary Rossby waves radiate away any pressure gradient along a PV contour; the net mass transport convergence in each layer where one ray changes layers is balanced by a net mass transport divergence in the same layer due to another ray with the same frequency. These continuity arguments suggest that the surface intensified flow that will be excited by a bottom-intensified flow is approximately twice as strong as the surface projection of the bottom-intensified flow, and similarly for the excitation of bottom-intensified flow. Since the very low frequency waves are extremely surface or bottom intensified, the strength of the coupling between layers decreases with decreasing frequency. The localized coupling suggested by the ray tracing, and the magnitude of the coupling based on these continuity arguments, are strongly supported by the primitive equation experiments.

One qualitative explanation for the localization of the coupling is that when the vorticity gradients of the two layers are in very different directions, there is a very weak expression of lower-layer intensified low-frequency flow in the upper layer, and vice versa. The low-frequency flow is very much more intensified near or away from the bottom boundary than would be predicted by the Burger number 1 scaling that is found for  $f$ -plane topographic waves (Rhines 1970). The restoring force for the bottom-trapped topographic Rossby waves is the topographic vorticity gradient due to the bottom boundary. In fact, on an  $f$  plane this is the only restoring force that leads to subinertial waves. [Kelvin waves are excluded by the bottom topography and even relatively weak (or realistic) stratification; they are replaced by the bottom-trapped topographic Rossby waves (Rhines 1970).] When variations of the Coriolis parameter are included, the planetary vorticity gradients act on the interior fluid as well. The bottom topography is typically such a strong restoring force that flow right at the bottom must be aligned with the isobaths, but when isobaths are not zonal any interior flow along isobaths is subject to a significant restoring force due to the planetary vorticity gradient. Conversely, low-frequency surface-trapped flow must be nearly zonal, but any flow across the bottom topography will be subject to a strong restoring force. The two incompatible constraints are accommodated by the free low-frequency waves becoming extremely bottom-intensified or having exceedingly small bottom velocities. The surface- and bottom-intensified flows are effectively detuned (Rhines 1977). When the isobaths are nearly zonal, the two constraints on the direction of low-frequency flow are consistent and the flow is much less bottom or surface intensified. Where the vertical distribution of energy of the surface- and bottom-intensified modes with the same frequency and nearly the same wavenumber coincide in space, there is a possibility of coupling between the modes.

The linear coupling between surface- and bottom-

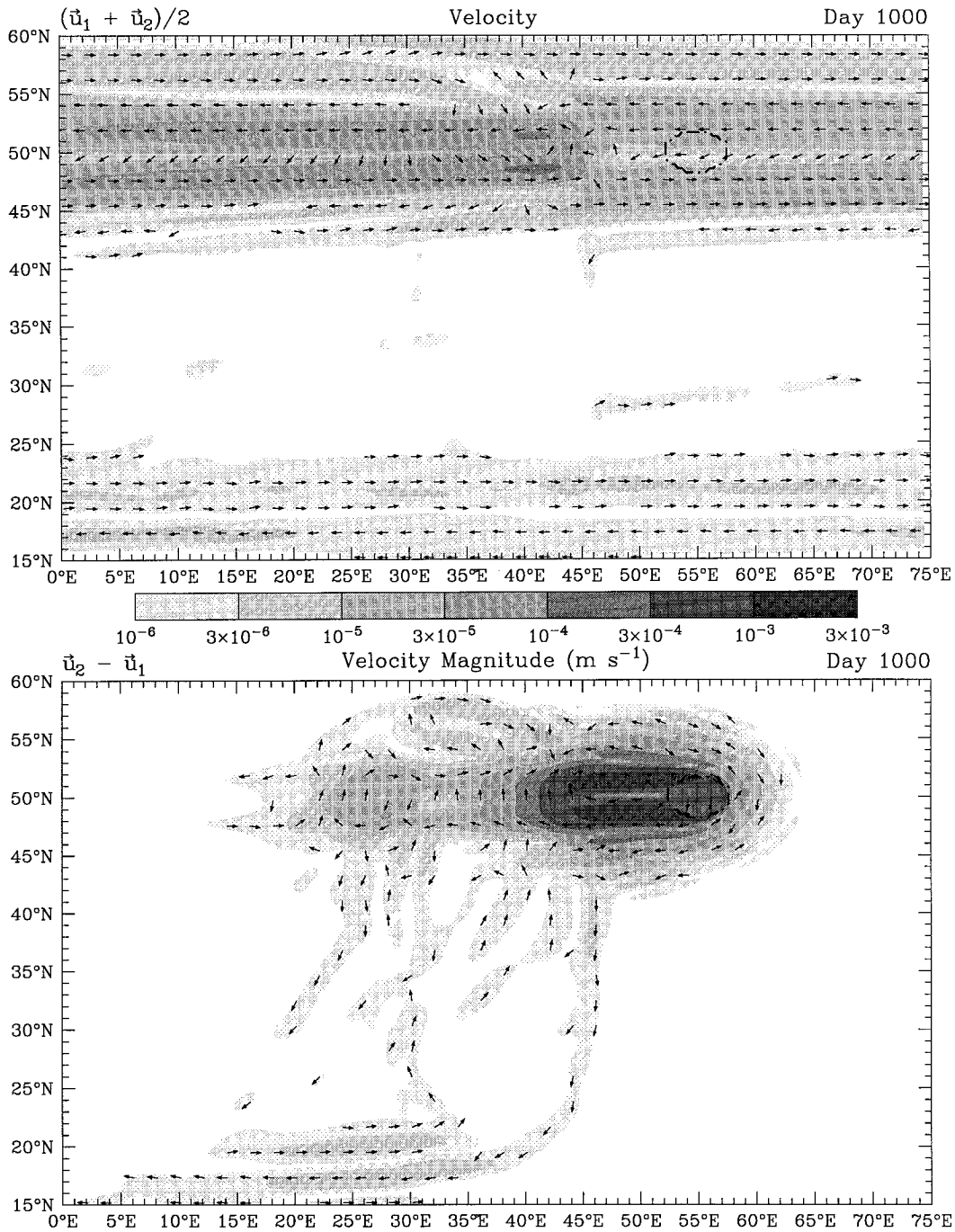


FIG. 14. The velocities at day 1000 of the four-layer simulation. The shading indicates the magnitude of the flow, while the vectors indicate the direction of flow. The dashed-dotted circle marks the forcing location. The first panel depicts the average velocity of the uppermost two layers.

intensified flow demonstrated in this paper has implications for our understanding of the reason for the abyssal flow. The ancient view of a “quiescent abyss” is clearly wrong. Crude theories of a sluggish directly forced abyssal circulation with the only strong flow at the boundary give some qualitatively correct predictions but may be misleading in ascribing a cause for the

boundary currents. It is only recently that hydrographic sections with an accurate “level of known motion” have become common. Velocities from earlier sections with an assumed “level of no motion” (usually in the deep!) are useless for describing the deep ocean circulation. Recent observations with an ADCP-derived reference velocity show a rich field of bottom-intensified topo-

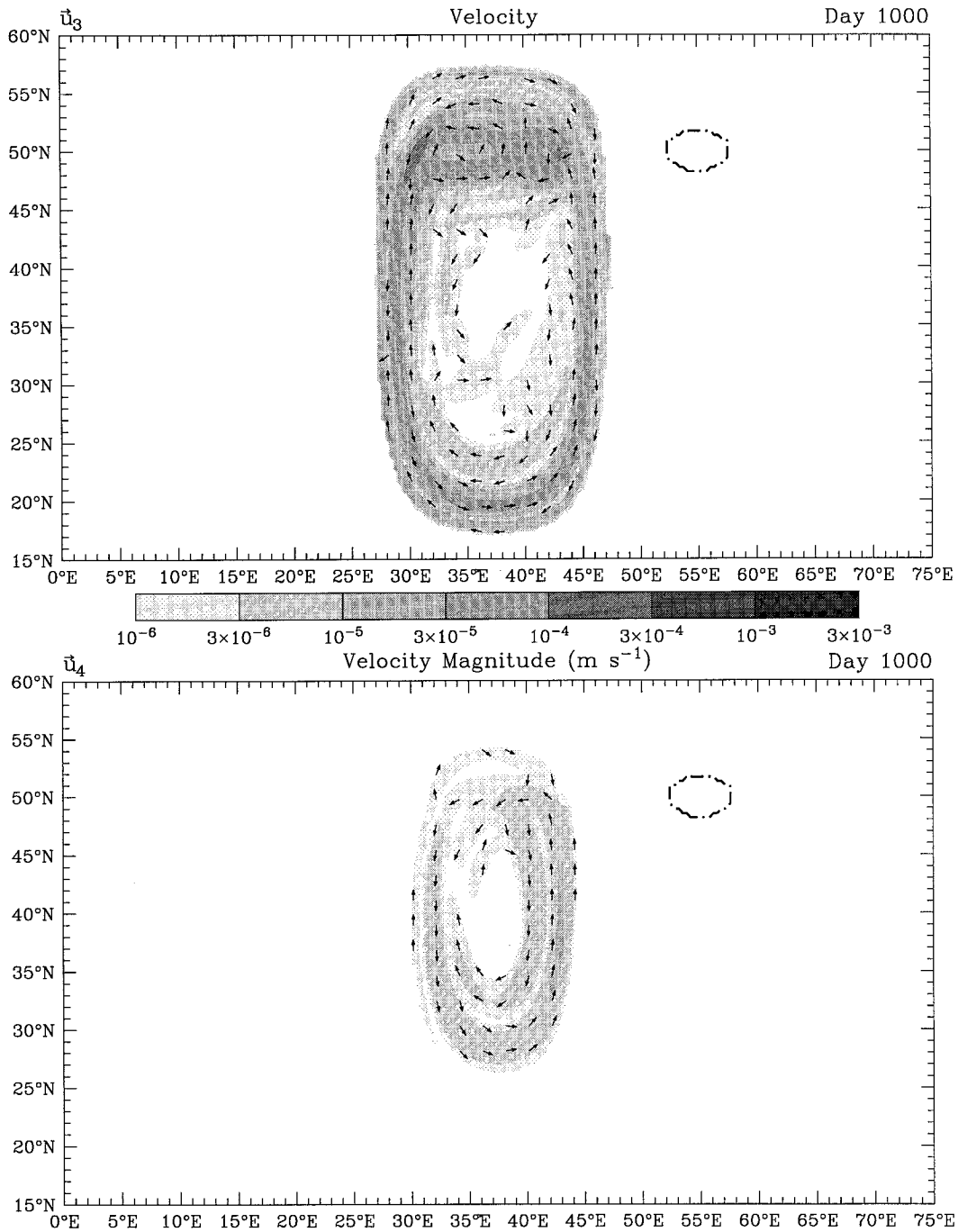


FIG. 14. (Continued) The second panel shows the velocity difference between the second and first layers. The velocities of the third and fourth layers are shown in the last two panels.

graphic Rossby waves off the east coast of North America (Pickart 1995).

The most important consequence of the coupling, described here, between surface- and bottom-intensified flow lies in the possibility for variability in the (surface intensified) wind-driven circulation to excite abyssal flow. Extremely strong surface currents flow past topography with an appropriate orientation in such places

as the Grand Banks and Cape Agulhas. It is entirely possible that abyssal circulation excited in these places might be quite important along the western margins of the North Atlantic and southern Indian Oceans. It must be emphasized that the coupling mechanism described here only operates at frequencies less than the maximum internal Rossby wave frequency. At high latitudes the small Rossby radius and planetary vorticity gradient re-

strict this coupling to very low frequencies. In more tropical regions, the maximum Rossby waves frequency is much higher, and the coupling even applies at annual frequencies. The Gulf of Guinea may be one place where a strong abyssal circulation is driven by the annual cycle of the surface circulation. An important distinction of the present coupling mechanism is that it is linear, as opposed to other nonlinear eddy forcing mechanisms for driving a deep circulation. This means that this coupling of the abyssal circulation to the surface applies anywhere where the topographic slope is in the right direction, regardless of the strength of the surface circulation and eddy field.

This study suggests a source for the deep flow in addition to direct forcing and nonlinear eddy forcing. It is possible that linear coupling between the surface flow and bottom-trapped flow due to topography is responsible for some of the abyssal circulation in the ocean. Because this forcing mechanism is linear, it can drive flow in either sense. By contrast, direct forcing due to upwelling always tends to drive cyclonic sense flow around either an isolated depression or plateau (Kawase and Straub 1991), and dissipation of topographic Rossby waves tends to drive a pseudowestward flow (Thompson 1995). Further, this study demonstrates that this coupling is localized in regions of parallel or antiparallel topographic and planetary vorticity gradients. The fact that this mechanism for driving the deep flow is linear and localized may help explain some of the variability in the observed deep ocean circulation.

*Acknowledgments.* I would like to thank P. Rhines for his support and valuable guidance in this study. I would like to thank M. Kawase, L. Thompson, P. MacCready, and J. Allen for helpful discussions. K. Bryan and A. Gnanadeskian provided valuable internal reviews. Comments from two anonymous reviewers helped clarify the arguments. J. Sheldon and H. Vahlenkamp helped make one of the figures. Most of the figures were made with the Ferret plotting package from NOAA PMEL. This work was supported by an ONR Graduate Fellowship, ONR Grant N00014-92-J-1405, a Visiting Scientist Fellowship from Princeton University, and a UCAR Ocean Modelling Postdoctoral Fellowship.

## REFERENCES

- Allen, J. S., 1980: Models of wind-driven currents on the continental shelf. *Annu. Rev. Fluid Mech.*, **12**, 389–433.
- , and R. D. Romea, 1980: On coastal trapped waves at low latitudes in a stratified ocean. *J. Fluid Mech.*, **98**, 555–585.
- Anderson, D. L. T., and A. E. Gill, 1975: Spin-up of a stratified ocean, with application to upwelling. *Deep-Sea Res.*, **22**, 583–596.
- , and P. D. Kilworth, 1977: Spin-up of a stratified ocean with topography. *Deep-Sea Res.*, **24**, 709–732.
- Hallberg, R., 1995: Some aspects of the circulation in ocean basins with isopycnals intersecting the sloping boundaries. Ph.D. thesis, University of Washington, 244 pp. [Available from University Microfilms, 1490 Eisenhower Place, P.O. Box 975, Ann Arbor, MI 48106.]
- , and P. B. Rhines, 1996: Buoyancy-driven circulation in an ocean basin with isopycnals intersecting the sloping boundary. *J. Phys. Oceanogr.*, **26**, 913–940.
- Kawase, M., 1987: Establishment of deep ocean circulation driven by deep-water production. *J. Phys. Oceanogr.*, **17**, 2294–2317.
- , 1993: Effects of a concave bottom geometry on the upwelling-driven circulation in an abyssal ocean basin. *J. Phys. Oceanogr.*, **23**, 400–405.
- , and D. Straub, 1991: Spin-up of source-driven circulation in an abyssal basin in the presence of bottom topography. *J. Phys. Oceanogr.*, **21**, 1501–1514.
- Lighthill, M. J., 1978: *Waves in Fluids*. Cambridge University Press, 504 pp.
- Mertz, G., and D. G. Wright, 1992: Interpretations of the JEBAR term. *J. Phys. Oceanogr.*, **22**, 301–305.
- Pickart, R. S., 1995: Gulf-stream generated topographic Rossby waves. *J. Phys. Oceanogr.*, **25**, 574–586.
- Rhines, P., 1970: Edge-, bottom-, and Rossby waves in a rotating stratified fluid. *Geophys. Fluid Dyn.*, **1**, 273–302.
- , 1977: The dynamics of unsteady currents. *The Sea*, Vol. 6, E. Goldberg, Ed., Wiley, 189–318.
- , and W. R. Holland, 1979: A theoretical discussion of eddy-driven mean flows. *Dyn. Atmos. Oceans*, **3**, 289–325.
- Stommel, H. U., and A. B. Arons, 1960: On the abyssal circulation of the world ocean—I: Stationary planetary flow patterns on a sphere. *Deep-Sea Res.*, **19**, 707–718.
- Straub, D. N., 1994: Dispersion of Rossby waves in the presence of zonally varying topography. *Geophys. Astrophys. Fluid Dyn.*, **75**, 107–130.
- Thompson, L., 1995: The effect of continental rises on the wind-driven ocean circulation. *J. Phys. Oceanogr.*, **25**, 1296–1316.
- Veronis, G., 1980: Dynamics of large-scale ocean circulation. *Evolution of Physical Oceanography*, B. A. Warren and C. Wunsch, Eds., The MIT Press, 140–183.
- Wajsbowicz, R. C., and A. E. Gill, 1986: Adjustment of the ocean under buoyancy forces. Part I: The role of Kelvin waves. *J. Phys. Oceanogr.*, **16**, 2097–2114.